EUJO-LIMMS - "EUrope-Japan Opening of LIMMS", the first EU laboratory in Japan – December 2011 to May 2016

The **L**aboratory for **I**ntegrated **M**icro **M**echatronic **S**ystems is an international research unit on MEMS and NEMS (Micro- and Nano-Electro-Mechanical Systems) operated in joint names of the French National Centre for Scientific Research and the Institute of Industrial Science of the University of Tokyo, where it is located in **Komaba Campus (II)**, Tokyo, Japan. LIMMS hosts French and Japanese scientists, either CNRS permanent researchers or post-doctoral researchers in host research groups at UT-IIS. The research projects developed in LIMMS are related to micro and nanosystems within three main axes: Advanced MEMS/NEMS, BioMEMS/Nanobiotechnology and Nanotechnology.

In 2010, within the framework of the international cooperation specific activities of FP7, the European Commission launched an INCOLAB call for proposals, to establish European laboratories in third countries such as Brazil, China, India, Russia, USA, and Japan. **CNRS** and the **Institute of Industrial Science of The University of Tokyo** therefore offered to open LIMMS to 3 European partners:

- **Ecole Polytechnique Fédérale de Lausanne (EPFL)**, Switzerland
- **University of Freiburg, Department of Engineering (IMTEK)**, Germany
- **Valtion Technical Research Centre of Finland (VTT),** Finland

EUJO-LiMMS, EUrope-Japan Opening of LIMMS, therefore became the **first EU laboratory in Japan,** from December 2011 to May 2016. Thanks to this success, the Japan Society for the Promotion of Science also awarded EUJO-LIMMS with a 5-years matching fund through its Core-to-core program for mobility costs from UTokyo-IIS to EU partners.

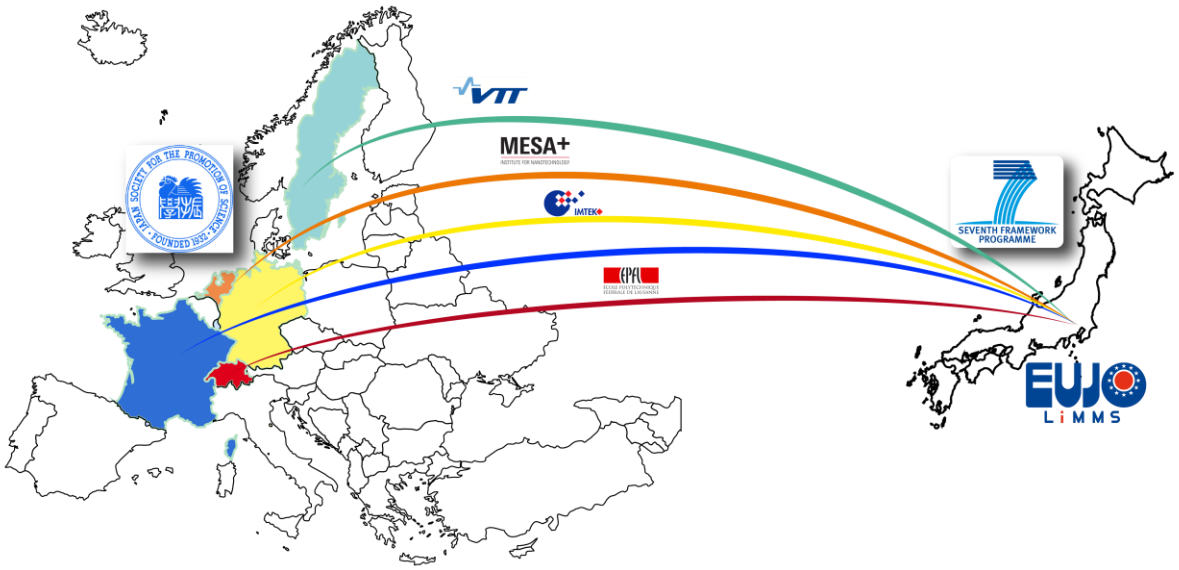

In 2013, EUJO-LIMMS organized an **open call for partner**. This is how in **April 2014**, EUJO-LIMMS opened up to one new partner: **MESA+, Institute for Nanotechnology of the University of Twente**, **Netherlands**, which was chosen among 11 excellent candidates.

The scientific challenge of EUJO-LIMMS is to **push the frontiers of micro and nano systems technology** in capitalising the complementary expertise of the UTokyo, CNRS and the four new European partners. The objectives of the project are therefore to extend the LIMMS structure and capacity to 4 European partners and study the feasibility to open the institutional agreement in the end of the project. Scientific projects are initiated between each partner and LIMMS as a first result of the creation of this EU laboratory. European researchers joined LIMMS members and the 16 Host laboratories of UTokyo where they could pursue their project in a collaborative environment.

LIMMS has been existing since 1995 and celebrated its 20th Anniversary in 2015. From December 2011 to May 2016, LIMMS developed its capacity in order to upgrade from a bilateral cooperation to a real European Laboratory, in terms of management, administration, administrative and technical hosting as well as research planning. EUJO-LIMMS successfully hosted **21** European Researchers, from EPFL, IMTEK, VTT and MESA+.

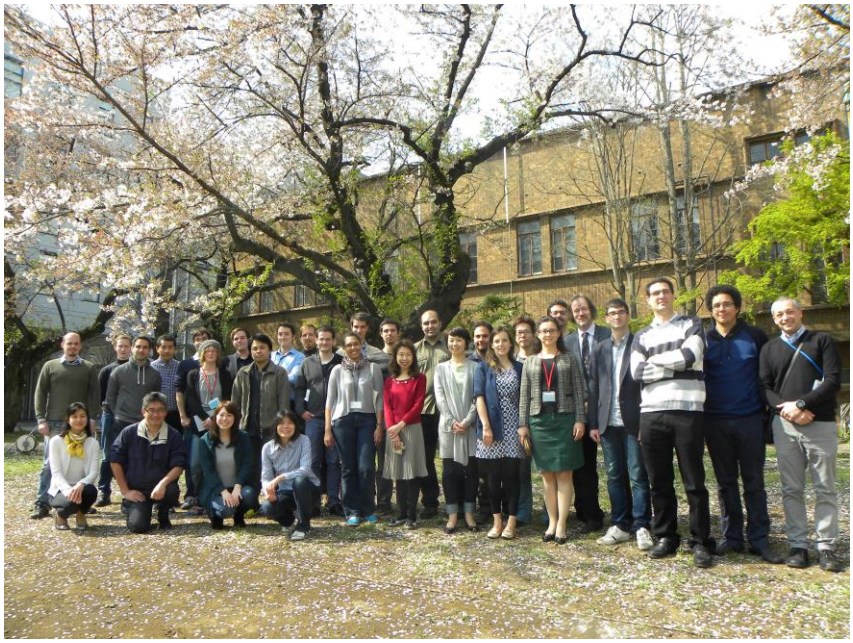

LIMMS and EUJO-LIMMS Members in 2015 at The University of Tokyo Institute of Industrial Science – Komaba Campus

When looking at the statistics we can see the EUJO-LIMMS project brought a significant increase in the hosting activity of the laboratory. Twenty-one researchers have been hosted in 4 years, some of them came for several stays, thus doubling the number of hosted researchers on the given period. A hosting and training strategy had to be implemented to be able to maintain and improve the quality of research for EU researchers. LIMMS has therefore selected a technical support team based on each project, and skills of the EU researchers. In terms of administration, LIMMS upgraded its hosting capacity, structure and documentation to meet the EU standards, and provided an efficient office support team for all matters related to a mobility to Japan. This 4 year-effort is a valuable asset for the future of the EU laboratory of Japan in the next years. The new EU laboratory communicated on its activities, first in view of the call for partner in 2013, then in view of ensuring the sustainability of the laboratory further to the end of the project.

Four Information Days and Workshops were organized in Japan, France, Switzerland, Germany and Finland.

The EUJO-LIMMS consortium gathered at CNRS, Paris, September 29, 2015 for the Final Workshop and Consortium meeting.

On the EUJO-LIMMS website developed in 2012, all news, science and technology results as well as researchers profiles and publications can be checked.

http://limmshp.iis.u-tokyo.ac.jp/about-the-laboratory/eujo-limms

One of the goals of the EUJO-LIMMS project was also to compare the institutional and administrative systems from each of the five EU institutes and study their compatibility with the current LIMMS at The University of Tokyo, as well as their strengths and weaknesses in order to build an international laboratory. A case study of these systems was therefore published and was used in the end of the project to release a **start up guide to creating a joint international laboratory**. The 20 years experience of LIMMS as a French-Japanese laboratory and its extension to EU partners was an excellent case to identify best practices that can be used by any future EU research institute interested in building long-term scientific cooperation abroad.

Scientific projects were initiated during these four years between each partner and LIMMS as a first result of the creation of this EU laboratory. European researchers joined LIMMS members and the 16 Host laboratories of UTokyo where they could pursue their project in a collaborative environment.

EPFL, Switzerland – LIMMS, Japan
COOPERATION

The cooperation between EPFL and LIMMS focused on "micro/nanofabrication of soft-matter MEMS / stretchable electronics" which was systematically investigated not only from fundamental fabrication mechanism but also in view of new practical applications. The research activities focus on the controllable 3D nanopatterning technology and developing cost-efficient advanced MEMS devices, specifically for lab-on-chip and microenergy applications. Three main topics were systematically investigated, including advanced 3D nanofabrication techniques based on thermal scanning probe lithography (TSPL) and advanced stencil lithography respectively, highly efficient and gentle trapping of single cells in large microfluidic arrays, and high performance triboelectric generator based on nature material of silk fibroin

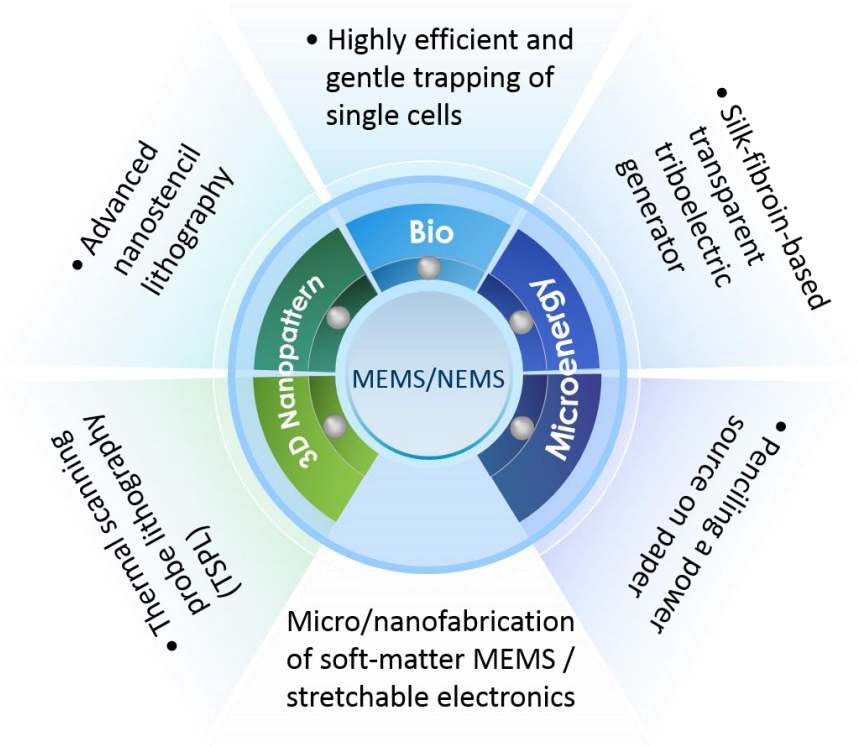

The above figure shows the brief summary description of WP3 objectives, including three main lines: advanced 3D nanopatterning techniques, new applications in biomedical and microenergy field.

MAIN S&T RESULTS/FOREGROUNDS of EPFL-LIMMS PROJECTS

EPFL-LIMMS 1. Thermal modification of poly-phthalaldehyde using micro heaters

1.1 Summary

We developed a method to pattern thermo sensitive polymer resists such as poly-phthalaldehyde or molecular glasses as a complementary method to thermal scanning probe lithography (TSPL). These types of polymers can be transformed into vapor phase upon heating. The method exploits joule heating to locally change the polymer phase.

1.2 Results and Discussion

Recent progresses involve the design of the microheater stamp and COMSOL simulations to study the heat distribution in the heater and the substrate and a proof of concept. A micrometer to nanometer sized heater is used to locally modify a temperature sensitive resist. In a second step, a thermal scanning probe is used to image the pattern and add nanometer sized features. According to COMSOL simulation results, the effect of a thermal insulation layer is studied in order to reach sufficiently high temperatures to decompose the resist when the heater is in contact with the substrate. As the results show, a thermal insulation layer allows for higher local temperatures around the heater in comparison to the stamp without a thermal insulation layer. Two checkerboard patterns were written into pristine poly-phthalaldehyde (left) and the pre-patterned resist (right). The cross section profiles confirm that additional patterning with a thermal probe is feasible on both structures. This is the first time mix and match thermal lithography on a single sample is demonstrated.

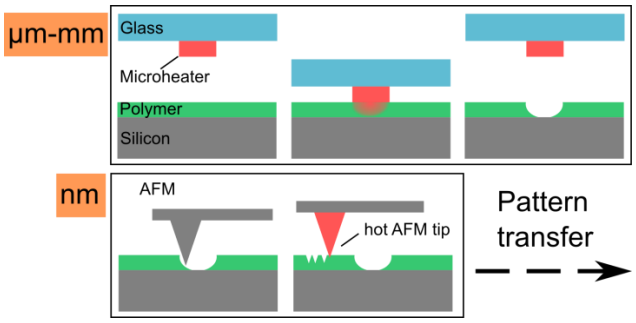

Figure 1.1: This sketch shows the basic principle of a mix and match lithography using a microheater in a first step to pattern a temperature sensitive resist with micro to mm sized patterns and in a second step using a thermal probe with a tip apex in the range of 20-50nm to add nanometer features.

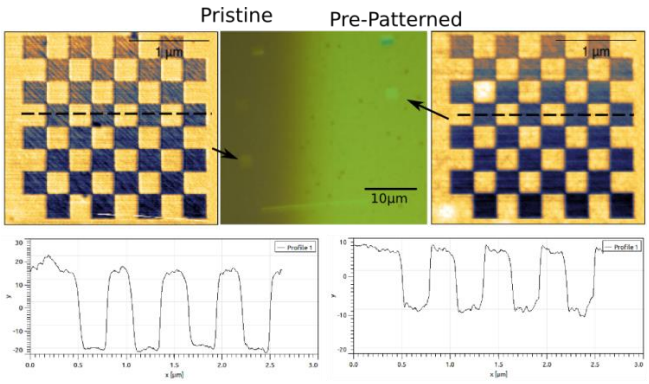

Figure 1.2: A checkerboard pattern written with a thermal scanning probe into pristine poly-phthalaldehyde (left) and thermally patterned resist (right). The corresponding cross sections show that mix and match thermal lithography is possible.

EPFL-LIMMS 2. Advanced stencil lithography

2.1 Summary

A new fabrication method for 3D metal nanostructures using high-throughput nanostencil lithography was developed. Aperture clogging, which occurs on the stencil membranes during physical vapor deposition, is leveraged to create complex topographies on the nanoscale. The precision of the 3D nanofabrication method is studied in terms of geometric parameters and material types. The versatility of the technique is demonstrated by various symmetric and chiral patterns made of Al and Au. This novel application of stencil lithography for the third dimension control on the nanoscale has great potential to pave the way for applications in many fields, such as photonics and bio-inspired materials.

2.2 Results and Discussion

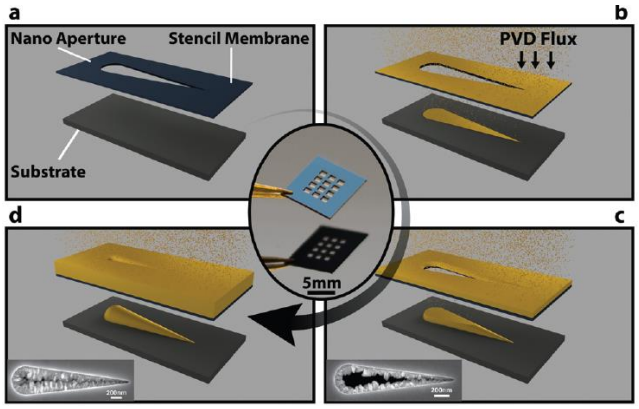

***Figure 2.1**: Stencil lithography clogging effect. (a) The stencil mask is assembled on a substrate using Kapton® tape. Three representative phases. (b) Initial phase: PVD occurs through the fully open aperture. (c) Intermediate phase: aperture is partially clogged. (d) Final phase: aperture is fully clogged and the final 3D nanostructure with a non-uniform height is formed. Insets show the SEM images of the apertures on the stencil membranes.*

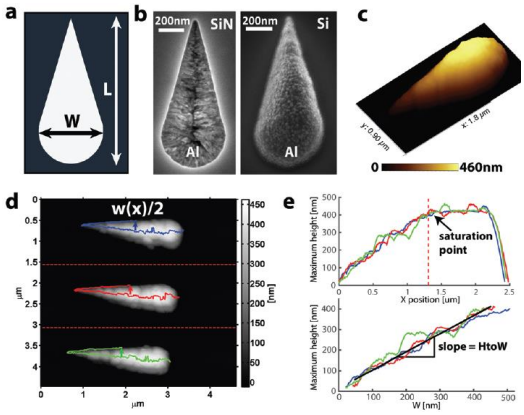

***Figure 2.2**: Width to height ratio characterization on the tapered line geometry. Top row describes the tapered geometry: (a) L and W. (b) SEM tilted (20°) image of a tapered structure (W/L=0.5µm/1µm). (c) AFM image. Bottom row describes the analysis performed on the AFM topography data to extract the relationship between the aperture width and the maximum height achieved: (d) and (e).*

We presented a novel use of stencil lithography to extend its applications to the height profile regulation that allows for the fabrication of 3D nanostructures with inhomogeneous thickness profiles. SEM and AFM acquired visual and topographical data is used to characterize the lithographic capabilities of our method. First, we quantified the clogging rate on various tapered line patterns by relating their AFM measured maximum height profiles to aperture widths and extracted the HtoW ratios as 1.69 for Au and 0.73 for Al. Our analysis of the AFM data showed no significant influence of the aperture dimension or geometry on the clogging rate; however, data revealed a strong material dependence. Moreover, we presented various patterns both with straight-four-pointed star and windmill-and curved-snail-geometric elements at different dimension scales, both with micron and submicron features, to illustrate the versatility and scalability of this approach, while discussing the resolution limiting aspects such as blurring and grain size dependence. Comparing individual windmill nanostructure profiles in an array, we were able to assess the homogeneity. The average profile standard deviations of arrayed windmill structures were measured

as 32 nm and 16 nm for Al and Au, respectively, which are affected by the average grain size of each material. This novel application of stencil lithography for the third dimension control on the nanoscale has great potential to pave the way for applications in many fields, such as photonics and bio-inspired material in life sciences, particularly in the cell-cell and cell microenvironment interaction, and cell heterogeneity research.

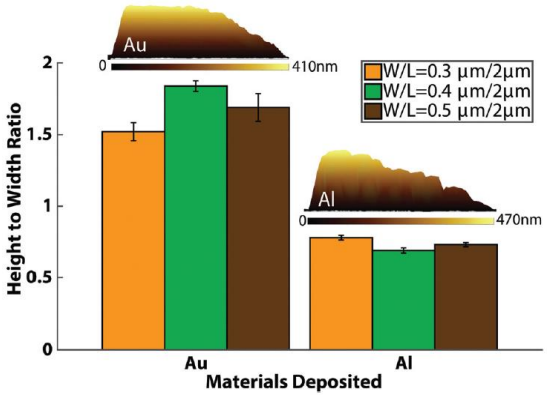

Figure 2.3: *HtoW ratio collected statistically on tapered structures with three different W/L ratios and for two different materials (Al and Au) showing significant material effect on the HtoW ratio but not as significant geometry dependence. Error bars represent the standard error over 12 samples for each tapered geometry.*

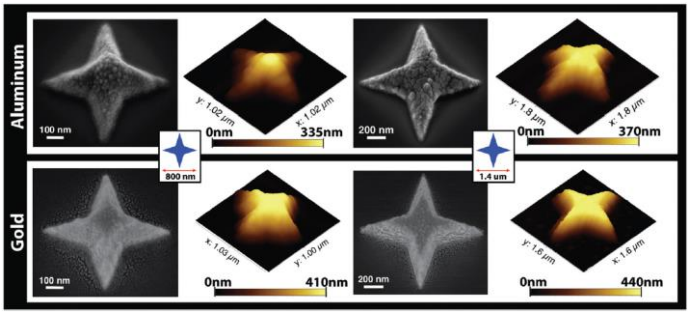

Figure 2.4: Scalability of the height control on a symmetric four-pointed star shape. Top and bottom rows show both the SEM images and the AFM topography of the four-pointed star shapes for Al and Au materials, respectively. The pattern is presented in two dimension scales: the smaller pattern on the left with 800 nm and the bigger pattern on the right with 1.4 µm total width. The average grain size of Al and Au can be compared on the SEM micrographs.

EPFL-LIMMS 3.Highly efficient and gentle trapping of single cells in large microfluidic arrays

1. Summary

The isolation of single biological cells and their further cultivation in dedicated arrayed chambers are key to the collection of statistically reliable temporal data in cell-based biological experiments. In this work, we present a hydrodynamic single cell trapping and culturing platform that facilitates cell observation and experimentation using standard bio-lab equipment. The proposed design leverages the stochastic position of the cells as they flow into the structured microfluidic channels, where hundreds of single cells are then arrayed in nanoliter chambers for simultaneous cell specific data collection. Numerical simulation tools are used to devise and implement a hydrodynamic cell trapping mechanism that is minimally detrimental to the cell cycle and retains high overall trapping efficiency (~70%) with the capability of reaching high fill factors (>90%) in short loading times (1–4 min) in a 400-trap device. A Monte Carlo model is developed using the design parameters to estimate the system trapping efficiencies, which show strong agreement with the experimentally acquired data. As proof of concept, arrayed mammalian tissue cells (MIA PaCa-2) are cultured in the microfluidic chambers for two days without viability problems.

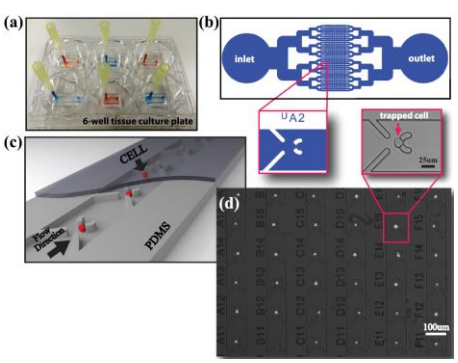

Figure 3.1: (a) Photograph of various microfluidic cell-trapping devices. (b) Typical 2D layout of the 32-channel device and a representative cell trap/chamber. (c) 3-D rendered model of the hydrodynamic single-cell isolating structured microchannel where the cells are sequentially trapped. (d) Fluorescent microscope image of the Calcein acetoxymethyl ester stained MIA PaCa-2 cells right after being arrayed.

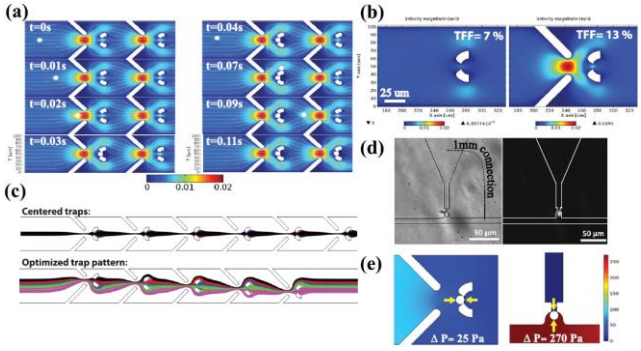

Figure 3.2: (a) FEM simulation. (b) An increase in the flux into the trap from 7% to 13%, which corresponds to the single trap capturing efficiency. (c) Trap position pattern in the channel. Top: all traps aligned at the center. Bottom: trap positions are optimized to target a wider (44%) range of streamlines. (d) and (e) A comparison of the proposed cell-trapping method with the reported serpentine-like.

2. Results and Discussion

In response to the growing need for manipulating single cells in microfluidic platforms, we designed, fabricated, and verified hydrodynamic single cell trapping and culturing devices. Our main goals were simplicity, high trapping efficiency, low mechanical intervention, short cell loading time, long-term microscopic observation compatible with stage-top incubators, and biological experimentation compatibility to facilitate the use of the method with standard bio-lab tools. We achieved ~70% trapping efficiency leveraging the stochastic nature of the cell arrivals in a microfluidic channel. Our average cell loading times were in minute scale (1–4 min). We cultured ~400 isolated single cells per device and monitored them using a stage-top incubator microscope. We did not observe any viability issue during the day-scale (~2 days) static cell culture periods. Moreover, we measured the time dependent proliferation rate of 73 individual MIA PaCa-2 cells (doubling frequency=0.8 day^{-1}), which was comparable with the control bulk cell culture proliferation rate (doubling frequency=1.1day^{-1}). We are convinced that our single cell microarraying method will stimulate and open the way to the studies of many biological questions

EPFL-LIMMS 4. High-performance triboelectric generator based on natural materials

1. Silk-fibroin-based triboelectric generator

In this work, a silk fibroin film material was introduced and used to construct a TEG. The silk material occupies a top-level positive position in the triboelectric series and possesses a strong ability to lose electrons during triboelectrification. An oxygen plasma treatment process was employed to strengthen the interface force via chemical modification and increasing surface roughness at the nanoscale level, and thereby improve the adhesion of the silk fibroin film to the PET substrate. Following a systematic study of its electrical property, this silk-based TEG was

demonstrated to be an efficient and reliable power source. The output performance of the fabricated TEG was very stable according to the results of a continuous test of 18000-cycles and a 3-week long-term test without failure. The benefit of using silk fibroin to construct TEG was proven by comparing it with other common triboelectric materials. The effect of environmental humidity to output performance of silk-based TEG was also studied. Finally, the maximum voltage, current, and power density to a match load of 40 MΩ achieved 268 V, 5.78 μA, and 193.6 μW/cm^2, respectively. In addition, it is worth mentioning that this silk fibroin material has two unique properties: controllable water solubility and transparency, which facilitate the realisation as wearable and ultra-transparent TEGs for future self-powered microsystems. Finally, the silk-based TEG was successfully utilised to independently operate two 4-bit LCDs and actuate a micro-cantilever, which extends the application field of TEG closer to practical applications.

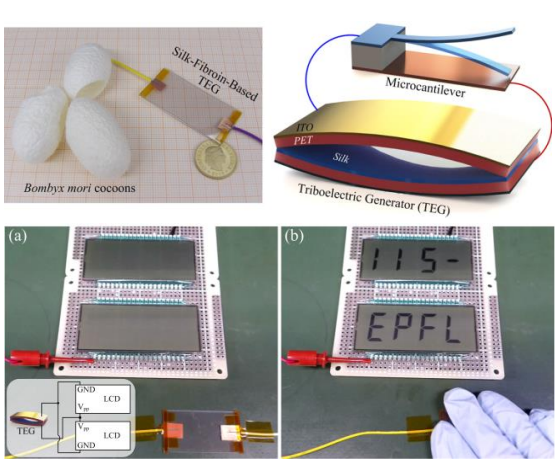

Figure 4.1: Photograph of the silk-based triboelectric generator (upper left), and cross-section microscope image of its bottom layer (upper right). Two 4-bit liquid crystal displays were successfully directly driven by the silk-based triboelectric generator (TEG) without any external circuit: (a) LCD off state, and (b) LCD on state.

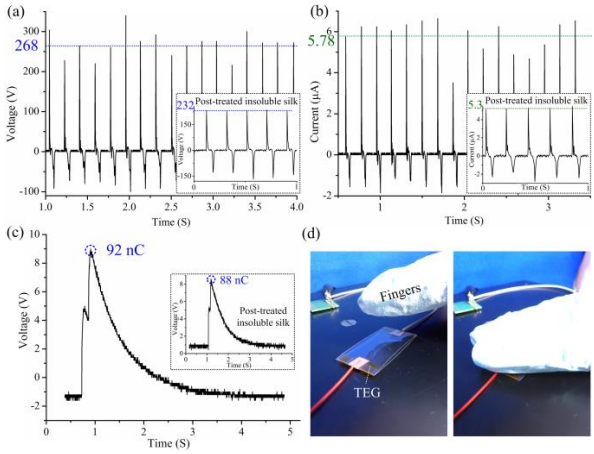

Figure 4.2: Electrical measurement of the silk-based TEG by ~5 Hz body motion (i.e., finger pressing): (a) output voltage and (b) current on the match load of 40 M□; (c) voltage of a 10 nF capacitor connecting with TEG via a full-wave rectifier bridge, which indicates the amount of charge transferred in one cycle; (d) driving the TEG by finger.

2. Paper-based triboelectric nanogenerator

We present a novel triboelectric nanogenerator (TENG) based on a paper-Teflon configuration fabricated by an easy and cost-efficient process. Carbon electrodes were hand-drawn by means of a graphite pencil on commercial paper cards, and the conductivity was confirmed by a multimeter. In order to increase the effective triboelectric area, we used sandpaper imprinting to increase the surface roughness more than 2-fold compared to flat surfaces yielding a more than 6-fold enhancement of power density. The achieved output voltage, current and power density were ~55 V, ~2.5 μA and ~17 μW/cm^2, respectively. The arch-shaped TENG shows robust output power when pressed by fingers to power a 2-bit liquid crystal display (LCD) demonstrating its use as energy harvester based on low-cost, commodity materials such as paper, Teflon and graphite.

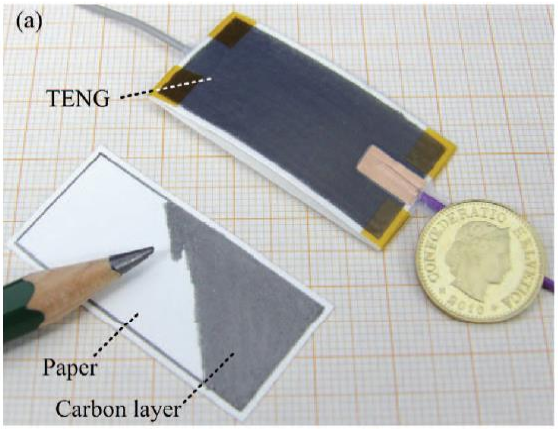

Figure 4.3: Photograph of paper-based triboelectric nanogenrator. Paper Cards were utilized as one material of triboelectric pair and as supporting structures. One of these two paper cards was covered by Teflon tape, which served as the other material of triboelectric pair.

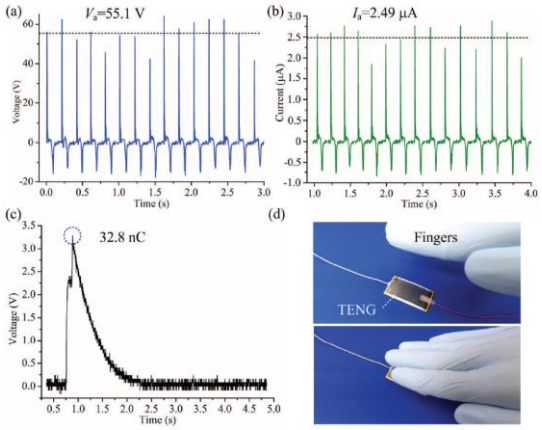

Figure 4.4: (a) Output voltage and (b) current of TENG on a matched load of 20 M□ (c) voltage of a 10 nF capacitor connected to TENG via a full-wave rectifier bridge, which indicates 32.8 nC charges transferred in one cycle; (d) test photograph by finger pressing (5 Hz).

POTENTIAL IMPACT of EPFL-LIMMS PROJECTS

As for 3D nanopatterning based on thermal scanning probe lithography (TSPL)

Thermal scanning probe lithography has shown its superior capability to produce 3D pattern in polymeric resists at high speed through interaction of the hot probe with the thermoresponsive polymer. It is possible to combine micro- to millimeter scale thermal patterning using a microheater and subsequent thermal scanning probe lithography to pattern the same temperature sensitive resist.

As for 3D nanopatterning based on nanostencil lithography

A new use of stencil lithography is proved to extend its applications to the height profile regulation that allows for the fabrication of 3D nanostructures with inhomogeneous thickness profiles. This novel application of stencil lithography for the third dimension control on the nanoscale has great potential to pave the way for applications in many fields, such as photonics and bio-inspired materials.

As for high-efficient and gentle single cell trapping

The following goals are successfully achieved, i.e. simplicity, high trapping efficiency, low mechanical intervention, short cell loading time, long-term microscopic observation compatible with stage-top incubators, and biological experimentation compatibility to facilitate the use of the method with standard bio-lab tools. We are convinced that our single cell microarraying method will stimulate and open the way to the studies of many biological questions in life sciences, particularly in the cell-cell and cell microenvironment interaction, and cell heterogeneity research.

As for high-performance triboelectric generator based on natural materials

In order for new green power sources – triboelectric generator (TEG) to make an impact in real life applications, further improvement is needed in particular in the choice of the pair of electrification materials beyond the choice of traditional materials that have been employed in the construction of TEGs. Here, under this project of WP3, we systematically studied and successfully introduced two

natural materials to construct high-performance TEG. Firstly, Silk fibroin was introduced as a novel material for TEG that occupies a top-tier position in triboelectric series. Silk fibroin was proven to be a promising material for TEG by comprehensive study and systematical test. Silk fibroin brings two advantageous potentials to TEG: >90% optical transmittance and controllable solubility. First demonstration of TEG successfully applied to sustainably power a mechanical micro-device (i.e., microscale cantilever). Secondly, a novel triboelectric nanogenerator (TENG) based on a paper-Teflon configuration fabricated by an easy and cost-efficient process. The novel approach based on triboelectric pair of paper-Teflon shows an attractive potential of producing commercial TENGs based on papers, a natural material and thus environmentally friendly.

IMTEK, Germany – LIMMS, Japan COOPERATION

This work package established novel devices and technologies for neuroscience, namely flexible neural probes and methods for guided neural cell growth on substrates. This included the developments of two methods for interconnecting rigid miniaturized neural probes to flexible cables and for temporarily stiffening the resulting flexible structures using biocompatible polymers. Secondly, several technological methods helping to place cells in wanted locations and arrange them in designed configurations in two and three dimensions on flat and structured substrates were demonstrated.

Capitalizing on expertise of IMTEK and UTokyo, and its combination, the two joint projects IMTEK/LIMMS-1 and IMTEK/LIMMS-2 of WP4 had as their main objective to further the state of the art in MEMS for monitoring neuronal signals in the central nervous system and of individual cells. They aimed at establishing the scientific collaboration of the two institutes and to lay the basis for an expansion towards projects beyond EUJO-LIMMS.

The objective of project IMTEK/LIMMS-1 was to develop mechanically flexible smart intracortical neural probes with a large number of recording sites. CMOS-based chips provided by IMTEK were to be embedded in a flexible polymer backbone forming a slender shaft. The chips comprise large numbers of electrode sites selectable by a switching matrix. They were to be connected among each other by metal interconnections in the connecting joints.

The objective of project IMTEK/LIMMS-2 was to advance the state of the art in manipulating the geometric arrangement of cell populations. The goals was to enable neuroscientific investigations of cell activity of individual cells or cells connected to other cells in designed arrangements compatible with predefined technical substrates. For this purpose MEMS methods were to be developed that enable such cell manipulation by appropriate surface functionalization, geometric substrate preparation, or microfluidic methods.

MAIN S&T RESULTS/FOREGROUNDS of IMTEK-LIMMS PROJECTS

The two projects IMTEK-LIMMS-1 and IMTEK-LIMMS-2 were defined in close coordination among the participating partners (groups of Prof. O. Paul at IMTEK and of Prof. S. Takeuchi at UT-IIS. Collaborators F. Barz (Ph.D. student) and F. Larramendy (Postdoctoral fellow) were hired by IMTEK and delegated to UT-IIS for individual durations.

IMTEK/LIMMS-1. Flexible smart intracortical neural probes

Intracortical neural probes that combine high recording site density, an appropriate probe stiffness during insertion and an optimized mechanical flexibility during long-term intracortical recording as described in the Deliverable D4.1 have been developed using the processes outlined in Deliverable D4.2. Figure 1 shows a comparison of the novel neural interface with an established neural probe. In contrast to the conventional neural probe in Fig. 1(a), the hybrid probe in Figs. 1(b,c) exhibits an increased flexibility that is gained from a thin and slender polymer interconnect interfacing the rigid silicon (Si)-based electrode array residing in deep cortical regions. By substituting the 50-µm-thick Si shank of the probe inside the cortical tissue by a roughly 11-µm-thick polymer interconnect, the bending stiffness is significantly reduced.

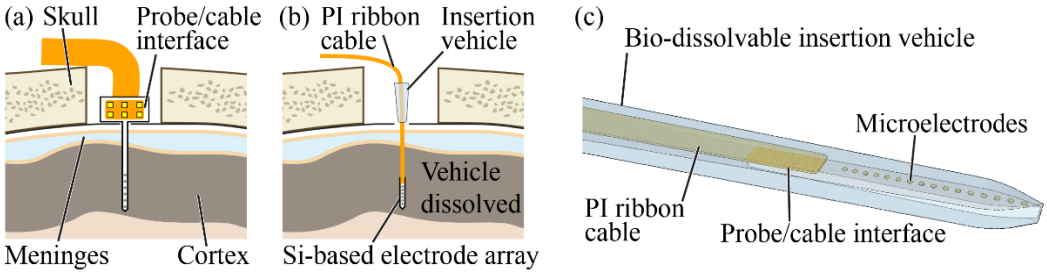

Figure 1: Schematic of (a) conventional and (b) flexible, hybridly assembled probe, and (c) flexible probe with insertion vehicle.

Electrode arrays as shown in Fig. 2(a) were fabricated using an established MEMS process relying on deep reactive ion etching (DRIE) and wafer grinding [3]. As a result, 50-µm-thick electrode arrays were released from a silicon substrate. Arrays with minimal width and length of 120 µm and 1.3 mm, respectively, carrying 16 or 32 electrodes were realized. To implement the slender probe shape, the bond pad dimensions at the probe/cable interface had to be reduced to 26 µm edge length and 34 µm spacing and the bonding parameters had to be adapted. Electrical properties of the electrodes are similar to those of conventional probes of IMTEK as they are based on the same basic fabrication processes.

The PI ribbon cables (thickness ca. 11 µm, {Fig. 2(b)}) comprise two platinum (Pt) metal layers sandwiched between three polyimide layers. A similar width of the cables and their Si counterparts was achieved. The high channel density in the region of the bond pads {cf. Fig. 2(b)} required the implementation of a plasma etching process. Lowered insulation resistance values after patterning of the metallization by means of argon plasma etching were found. They may be attributed to metal residues and chemical changes of the substrate. A subsequent treatment of the samples after sputter etching by oxygen plasma improved the electrical insulation.

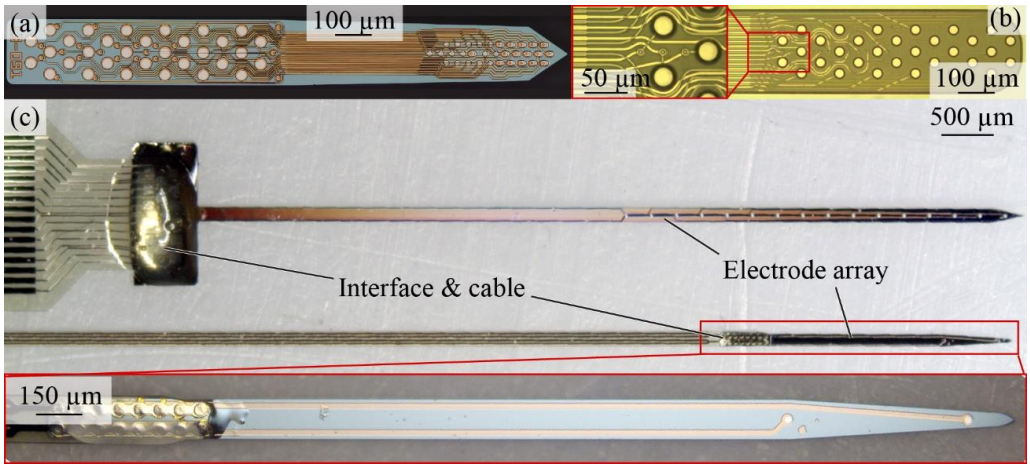

Figure 2: Micrographs showing fabrication results of (a) electrode array, (b) dry etched PI cable and (c) test structure of the flexible probe compared to a conventional neural probe.

An alternative wafer-level process for the interconnection of ultrathin silicon chips was also implemented using a novel handle wafer concept. The concept addresses the difficulties in aligning of the probes and planarizing the handle wafer surface for the subsequent electrical interconnection of chips and cables. It furthermore facilitates the final device release.

Figure 3(a) shows the schematic of a flexible probe with two electrode arrays interfaced by a polymer interconnect. The parylene-C-based process aims at the realization of such probes using the CMOS-compatible used for silicon probe fabrication at IMTEK. As outlined in Fig. 3(b), thin electrode arrays are fabricated from standard Si substrates and then embedded into the shellac matrix. The resulting composite handle wafer then serves for the cable fabrication directly on top of the embedded chips. Finally, the polymer matrix is dissolved in boiling ethanol.

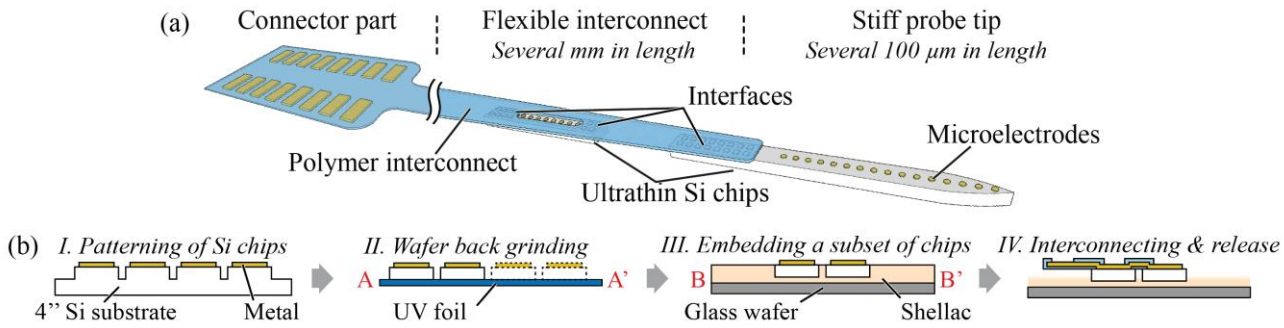

Figure 3: Schematic of (a) multi-chip neural probe of reduced foot print and (b) process flow of the demonstrated shellac-based interconnection process.

Finally CMOS probes suitable for the flexible probe assembly described above were designed and fabricated. For fabrication we used a 0.18 2P6M CMOS process of X-FAB Erfurt. This was then followed by the standard process developed at our group for turning the CMOS substrates into neural microstructures. These slim probes comprise up to 72 recording sites connected to a switching matrix enabling one to configure a large number of recording site patterns.

The project led so far to publications at the IEEE MEMS 2015, the Eurosensors 2015 and the IEEE MEMS 2016 Conferences (authors: F. Barz et al.).

IMTEK/LIMMS-2. Chip for parallel cell monitoring

First we report the fabrication, functionalization and testing of SU-8 microstructures for cell culture and positioning over large areas. The microstructure consists of a honeycomb arrangement of cell containers interconnected by microchannels and centered on nanopillar arrays designed for promoting cell positioning. The containers have been dimensioned to trap single cells and, with a height of 50 µm, prevent cells from escaping. Examples of microstructures populated by PC12 neuronal cells are shown in Fig. 4. [F. Larramendy et al., J. Micromech. Microeng., 2015]

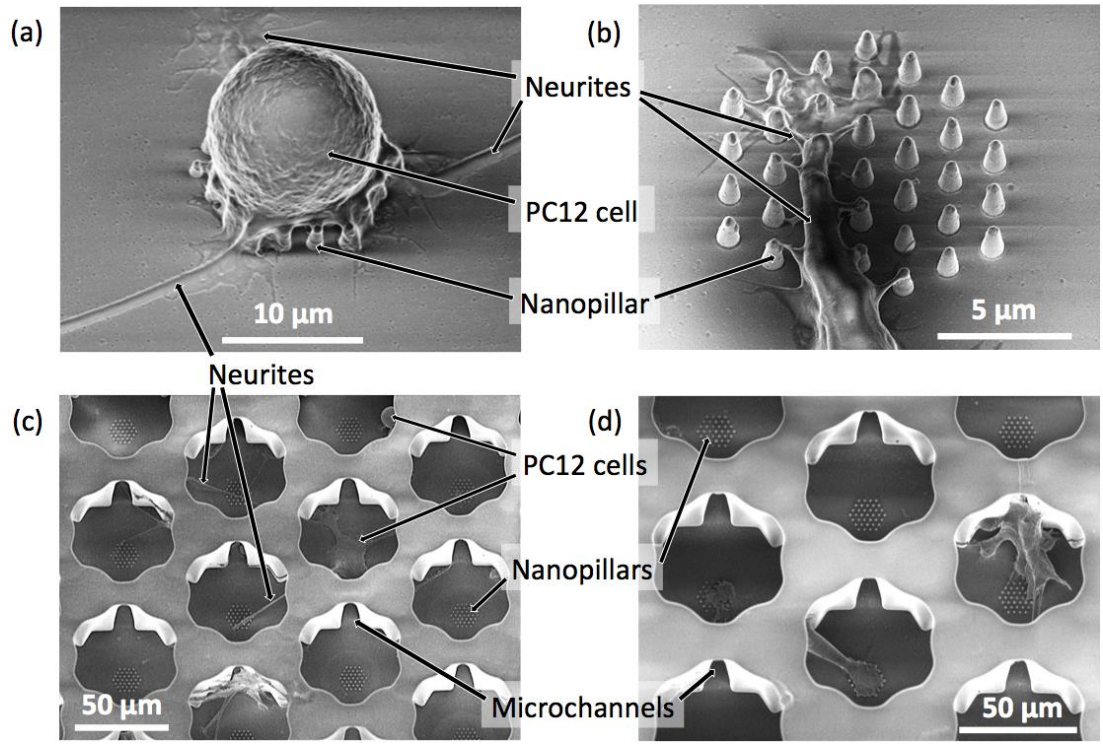

Figure 4: Scanning electron micrographs of (a) a neuron sitting on a nanopillar array with neurite growth, (b) a cell attached with several neurites to a nanopillar array, and (c,d) neurons pre-positioned on nanopillar arrays by a honeycomb arrangement of cell containers, with neurites extending across microchannels.

Secondly, a method to achieve the surface modification of substrates exhibiting pronounced topographies with recessed and protruding microstructures was developed. The method allows to produce patterns of delicate molecules such as laminin on such substrates. Patterns comprising arbitrary networks of modified and unmodified areas are thus possible {Fig. 5(b)}. The technique is based on the peel-off of a parylene-C template conformally deposited on a structured sacrificial photoresist. The parylene layer serves the combined purpose of a mask and a structural material: on the one hand it locally protects the substrate by direct contact; on the other hand, by bridging over the photoresist, it interconnects all protection patches into a continuous layer {Fig. 4(c)}. The substrate is ready for surface modification as soon as the sacrificial photoresist has been dissolved {Fig. 5(c)}. After surface modification, the parylene layer is straightforwardly peeled off

{Fig. 5(d)}. Thereafter the area complementary to the first surface modification (no. 1) pattern can be modified differently (no. 2), e.g. using cell-repellent bovine serum albumin [F. Larramendy et al., IEEE MEMS Conf., 2015].

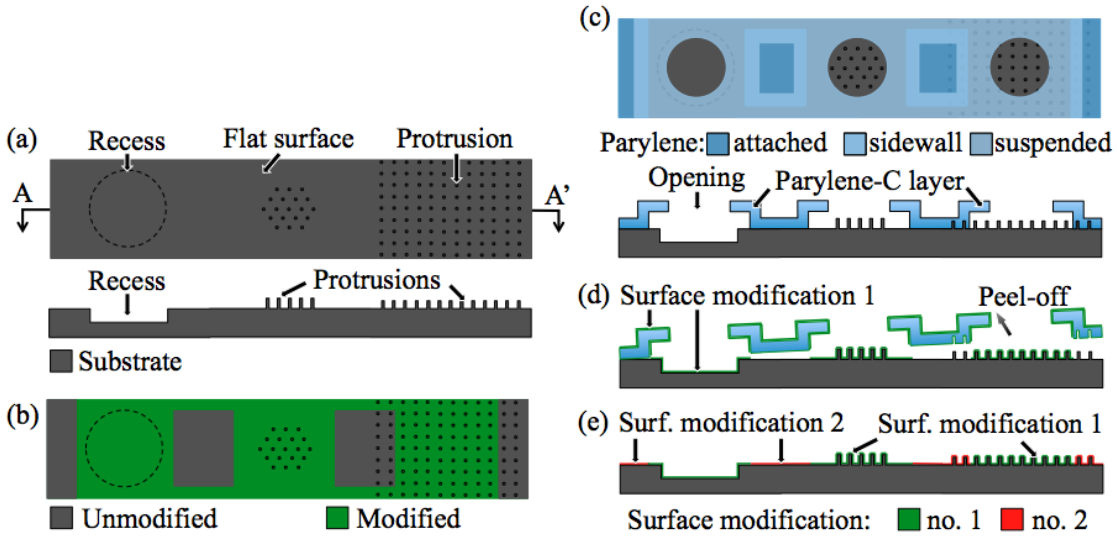

Figure 5: Concept of the parylene-C-based surface modification of substrated with pro-nounced topographies.

A further approach aimed at creating controlled cell culture networks in 3D. The technique is based on stacking cage-like microscaffolds, each scaffold containing cells. The scaffolds are produced in SU-8 photoresist using direct laser writing, a two-photon process as made possible by equipment of *Nanoscribe GmbH*, Germany. It was successfully demonstrated that neuron-like PC12 cells grow on such structures and establish cell-cell connections, and that cell-populated microstructures can be stacked, cf. Fig. 6. [F. Larramendy et al., Transducers Conf., 2015]

Finally, we introduced and demonstrated a technique for creating three-dimensional (3D) flexible microfluidic structures by a method inspired by the Japanese art of origami. It is based on a single structured and foldable layer of parylene-C. The technique has several advantages: (i) It requires few technological steps and does not rely on complex equipment, (ii) complex and small-size microfluidic systems are possible and (iii) multi-layer structures can be realized from a single starting layer. Selected examples of such folded multi-layer structures are shown in Fig. 7 [F. Larramendy et al., MicroTAS, 2015].

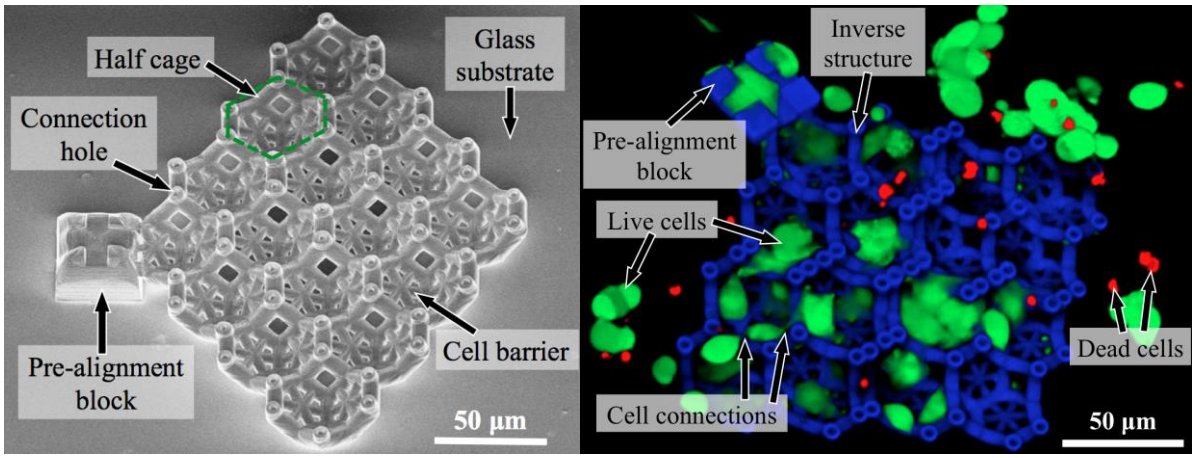

Figure 6: Scanning electron micrograph of an inverse structural layer formed of 16 half-cages and the fluorescence micrograph of this kind of microstructure after neuron-like PC12 cell deposition, three days of culture and a live-dead test.

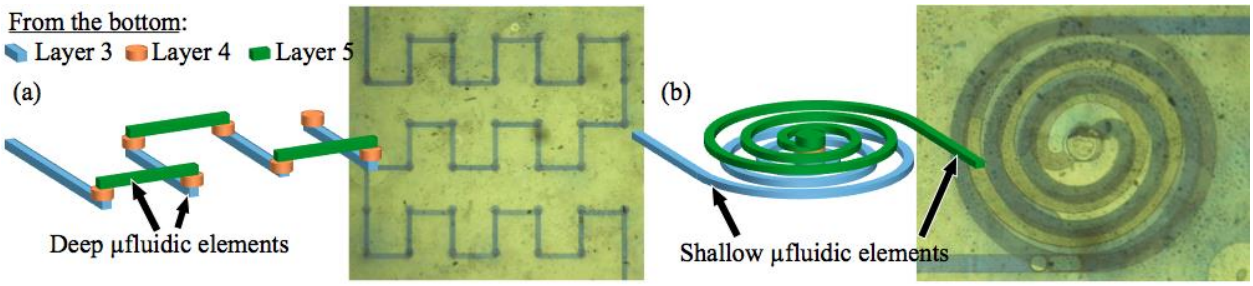

Figure 7: Optical micrographs and schematic 3D drawings of an ink test in (a) a 10-µm-wide daisy-chain of microchannels and (b) a two-layer spiral design realized in three different layers (nos. 3 to 5) with layer 1 serving as the support layer

POTENTIAL IMPACT of IMTEK-LIMMS PROJECTS

The results have a potential impact on the scientific community in that they enable new experiments in the area of life science to be designed. In the case of the results of Project IMTEK/LIMMS-1 these experiments may benefit from the achieved increased probe longevity in the brain under investigation. This is because tissue irritation is decreased due to the smaller dimensions of the probes and their ability to accommodate brain micro-motion, thus reducing the foreign-body reaction of the brain.

In the case of Project IMTEK/LIMMS-2 the increased flexibility in arranging neuronal cell into predefined configurations allows to carry out experiments on wanted arrangements of communicating neuronal cells and thus to study the dynamics of neuronal communication as a function of connection topology.

The ultimate benefit these tools and techniques aim for is the elucidation of still obscure mechanisms of brain dysfunction and the development of new approaches to curing these dysfunction or alleviating their symptoms. These are important issues for an ageing society where brains need to perform longer and longer, diseases such as Parkinson, Alzheimer, epilepsy, and stroke gain in importance, and the socio-economic burden caused by them grows.

VTT, Finland – LIMMS, Japan COOPERATION

This dedicated work packaged aimed at developing joint projects between VTT and LIMMS and to widen the scientific collaboration towards projects extension and new topics. Five researchers from VTT were seconded to Tokyo and carried out the research program. Dr. Kai Kolari did research at Prof. Fujii's laboratory at IIS for 4 months, Jan.-May 2012. During the visit he fabricated a microfluidic device to mimic human body and used it to test an influence of a prodrug on cancer cells. This research was done together with Dr. Kimura and Prof. Fujii from IIS. Dr. Tomi Haatainen worked at Toshiyoshi lab from September 2012 to March 2013. Dr. Tapio Mäkelä continued work from March 2013 to September 2013. During these 6+6 month periods, GHz MEMS metamaterial filter based on split-ring resonator device was designed and inkjet printing was used for demonstration. Focus was to show individual process steps. However, roll to roll manufacturing process could not be demonstrated totally. Basic principle of tune able version on electrostatic actuator top electrode on top of SRR element was introduced. LCC modelling showed 3 GHz shift in transmission peak by switching from OFF state to ON state in GHz device. The fabrication process using inkjet printing of metal dot array and spacers between top electrodes was optimised and flexographic method for printing bottom electrodes developed. (

Markku Kainlauri visited Kawakatsu lab from September 2013 until March 2014. He was carrying out experiments on graphene oscillators on the apex of a Pt tip. Platinum tips were successfully coated with graphene. First coatings were done at VTT using rapid thermal processing for tips sent from IIS. During his stay Mr Kainlauri and Mr Hidenobu Nishizawa modified Kawakatsu lab's tube furnace so that it could also be used for graphene deposition. Graphene coated tips were investigated using transmission electron microscope and scanning electron microscope.

Tommi Suni worked at Fujita lab from March 2014 until May 2014. The topic was TEM analysis on AlN thin films. The work started at VTT by preparing AlN thin films on silicon substrate using five different seed layer materials.

MAIN S&T RESULTS/FOREGROUNDS of VTT-LIMMS PROJECTS

VTT-LIMMS-1. Chip cell with high density connected microhabitats

Dr Kai Kolari did research at Prof. Fujii's laboratory at UTokyo for 4 months, Jan.-May 2012. This research was done together with Dr Kimura and Prof. Fujii from UTokyo.

In this work a microfluidic device was built to mimic human body circulation of lung cancer drug. In this device the prodrug was introduced to the system via thin membrane (intestinal cells), metabolized to actual drug in liver (area with liver cells) and transferred then to the lungs (area with lung cancer cells) via heart (micropump). Initial tests showed that HEPG2 could not be used in the experiments, as it was less resistant to Tegafur drug than A549 target cancer cells. Therefore primary HEP was chosen for main experiments. Within the time frame (48 hour exposure) it was difficult to see the effect of Tegafur or the combined effect of Tegafur and Uracil on the target

A549 cells in the microfluidic device.The staining method used in the work revealed only few dead cells and the result was about the same in the reference test without drugs. The concept may have the following restrictions;

1) PDMS may adsorb prodrugs or their metabolites more than a standard dish,

2) Time needed for A549 toxicity may be much longer than used in this study. Longer time could increase the effect on A549, but 48hours should be enough for the evaluation in general.

3) A549 survives in very low numbers in dish, without exchanging the medium for several days, making it very strong and independent cell type, thus a hard subject for proof of concept,

4) Staining may be limited in such a massive cell population as observed in the A549 chambers, possibly leading to misinterpretation of the viability of the target cells,

Possible solution: Optimizing the experimental conditions in future tests

5) The number of inoculated cells is very different in different microdevice due to inadequate mixing of cell suspension between the inoculations.

Possible solution is to optimizing the experimental conditions in future. In conclusion so far, we need to have some more time to optimize the whole set-up of the experiments to show our proof-of-concept. Especially for the cell culture experiments need much longer duration to achieve complete results.

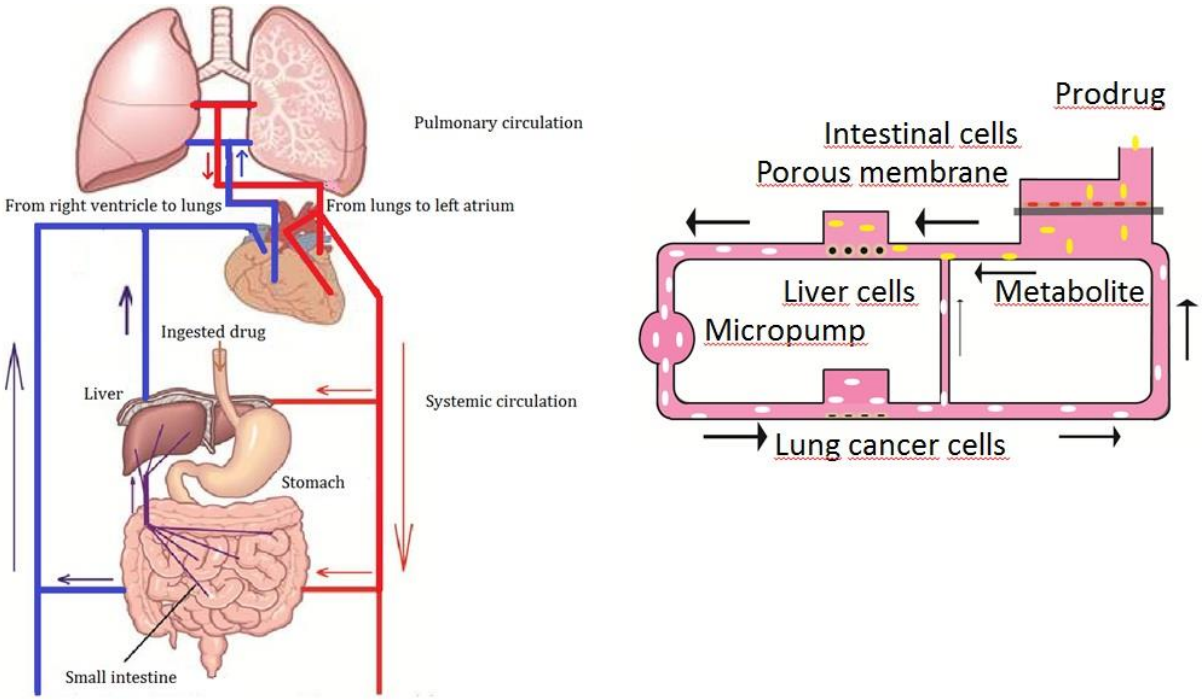

Figure 1. *The approach used in this work consisting of human body (left) that is mimicked by the analogue (right). The ingested prodrug enters stomach and small intestine, where is transported to systemic circulation. The capillary-transported prodrug enters liver and is metabolized. After metabolization the drug goes through heart and pulmonary circulation with the target lung cancer cells.*

VTT-LIMMS-2. MEMS Device for R2R Manufacturing

Dr. Tomi Haatainen worked at Toshiyoshi lab from September 2012 to March 2013. Dr. Tapio Mäkelä continued work from March 2013 to September 2013 (Deliverable reports D5.4a and D5.4b). During these 6+6 month periods, inkjet printing was used to design and demonstrate GHz MEMS metamaterial filter based on split-ring resonator.

During the first 6 months the device design was created and simulated. Plan for the MEMS metamaterial THz filter based on split-ring resonator was introduced. The function of the non-tunable version was simulated and also, first static (non-tunable) devices were fabricated on glass and plastic substrate using photolithography processes. In the next step, tunable version based on electrostatical actuator top electrode on top of SRR element was introduced. The function of the device was simulated by HFSS finite element method. The fabrication process using inkjet printing of metal dot array and spacers between electrodes was developed. The resolution of inkjet printer is not good enough to fabricate also the SRR structures by inkjet printing method.

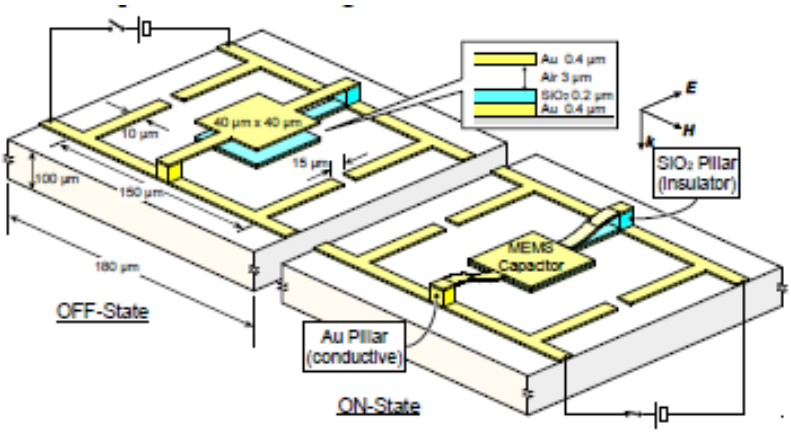

***Figure 2**. Unit cell of a tunable metamaterial THz filer with an electrostatic RF-MEMS capacitor (Zhengli Han et al, Toshiyoshi lab).*

High-frequency electromagnetic (EM) simulation using HFSS has been performed on the unit cell under the periodic boundary condition. The incident EM wave is set normal to the SRR with the electric field aligned in parallel with the MEMS capacitor bridge. The electrical current is confined within the capacitor bridge and that the electrical interconnections to the neighbour cells have little contribution to the RF coupling, thus maintaining the SRR resonance and allowing us to make a straight chain connection of cells to provide a route for the electrostatic MEMS operation DC voltage. The transmission spectrum of the device is shown in Figure 3.

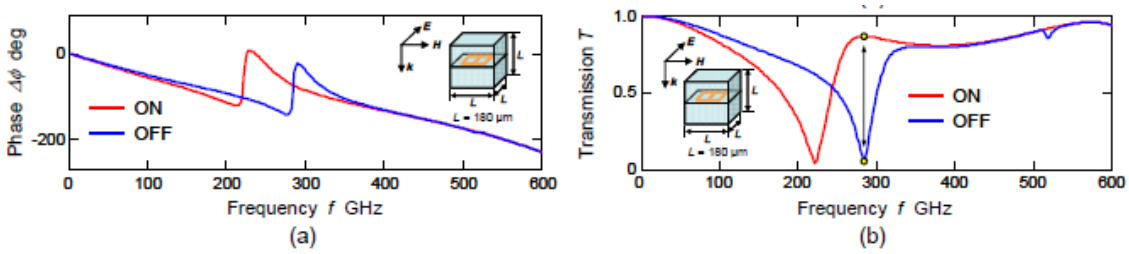

Figure 3. *Transmission spectra of the metamaterial THz filter with a MEMS tunable capacitor. (a) Phase shift through a 180-µm-tall cube and (b) transmission rate with resonance peak at 284 GHz (Zhengli Han et al, Toshiyoshi lab).*

Standard MEMS process was used transfer SRR patterns onto glass plate. First glass plate was sputter coated by 10 nm chromium to enhance adhesion of subsequent gold layer with thickness of 100-500 nm. The coated glass plate was spin-coated with S1818 photoresist which was exposed in mask aligner. After development the gold and chromium layer was removed by wet etching from the openings of the resist mask. In Figure 4 is shown the glass substrate with 100 nm gold layer and developed photoresist on top.

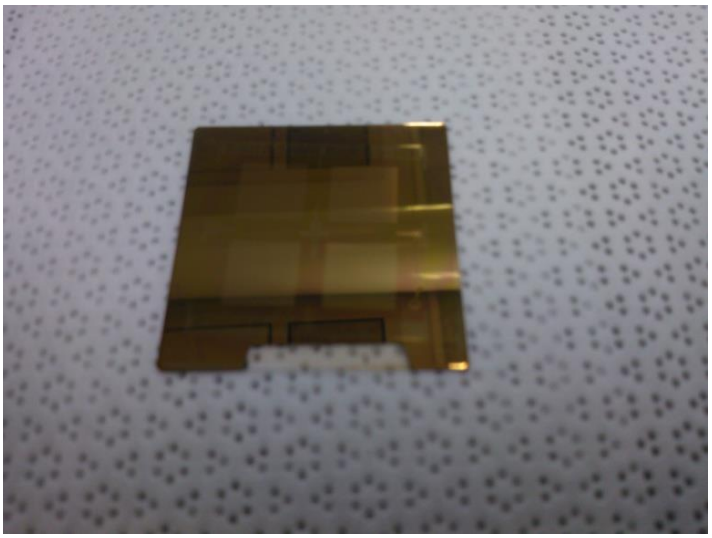

Figure 4. *Glass substrate with size of 40 mm by 40 mm coated with gold after exposing the photoresist.*

During the second 6 months period (by **Dr. T. Mäkelä**) inkjet printing was used to demonstrate GHz MEMS metamaterial filter based on split-ring resonator. We show individual process steps, but due to lack of roll to roll equipment, manufacturing process was not possible to demonstrate totally. Basic principle of tunable version on electrostatic actuator top electrode on top of SRR element was introduced. LCC modelling shows 3 GHz shift in transmission peak by switching from OFF state to ON state in GHz devise. The fabrication process using inkjet printing of metal dot array and spacers between top electrodes was optimized and flexographic method for printing bottom electrodes developed.

The resolution of inkjet printer limits to fabrication SRR structures in GHz region but it is suitable for GHz devices. Since at IIS, the imprint facilities are limited (e.g. hot embossing and roll to roll

equipment does not exist), flexographic method was developed and demonstrated. In the future more co-operations between IIS and VTT is essential if imprint facilities are decided to be used for device fabrication. SRR structure is not directly suitable for printing and therefore a novel design is needed. A parallel-plate capacitor size 40 µm x 40 µm, 3 µm gap and the square SRR pattern (180 µm x 180 µm) with an minimum feature size (4 µm cap) is difficult to achieve using printing techniques. Also aligning accuracy gives limitations to the design like this. Due to these reasons we propose a novel design suitable for inkjet and flexographic printing (Figure 5). Bottom electrode is printed on 125 micron thick polyethylene naphthalate (PEN) film when the top electrode is printed on 16 micron PEN film. 5 micron thick inkjet printed spacer (S1805 resist from Shipley) is used for separating PEN films from each other. Temperature (110oC, 10 min) and small pressure is used to attach the PEN films together. In this case spacer also works as glue between films.

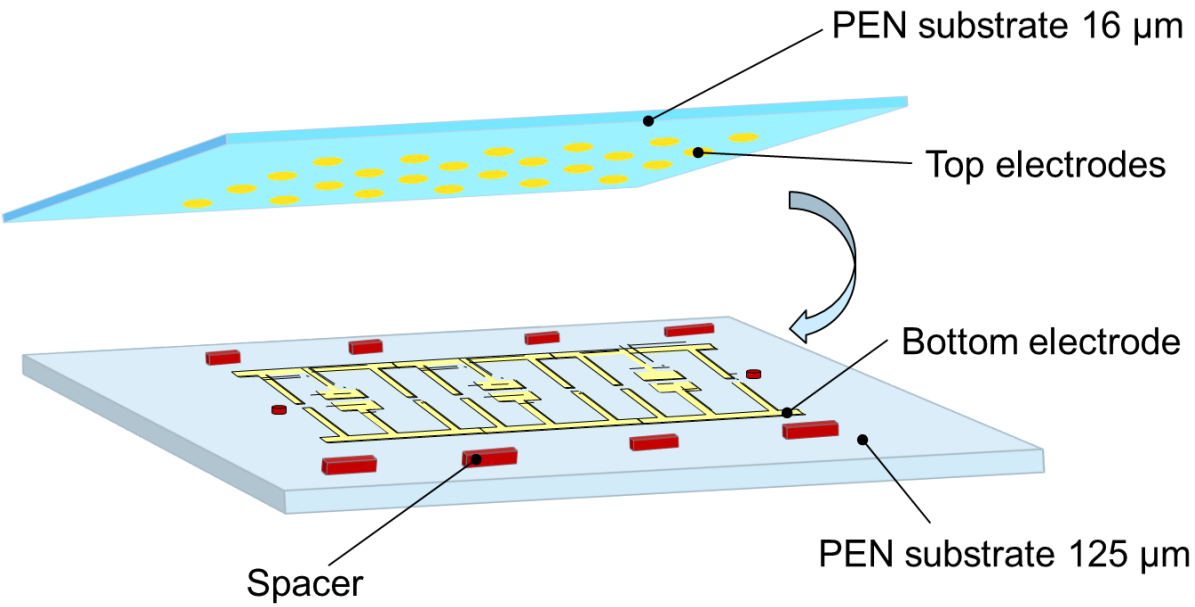

Figure 5. *Schematic principle of printable MEMS device. Bottom electrode is printed on 125 micron thick polyethylene naphthalate (PEN) film when the top electrode is printed on 16 micron PEN film. 5 micron thick inkjet printed spacer (S1805 resist from Shipley) is used for separating PEN films from each other.*

Electrostatic force is used to drive device and due smaller thickness of upper film it bends as shown in the Figure 6. In this design no electrical contact to the upper electrode is needed.

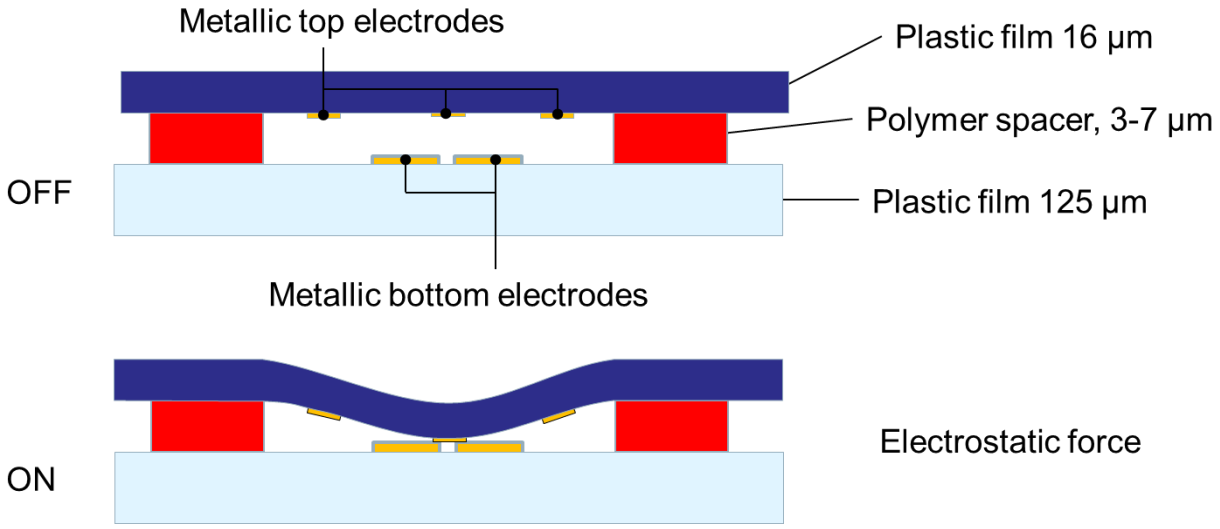

***Figure 6**. Electrostatic control of MEMS device. The top electrode is printed on 16 micron PEN film and therefore only upper film is moving in operation.*

Final device is seen in Figure 7 where SRR E MEMS device (A2_GHz) consist 16 unit cells. This printed MEMS device shows that inkjet printed devices are possible to fabricate. Characterisation in will be done in the future projects when characterization tools are ready to use. Inkjet printing method is limited to GHz devices due to the resolution limitation.

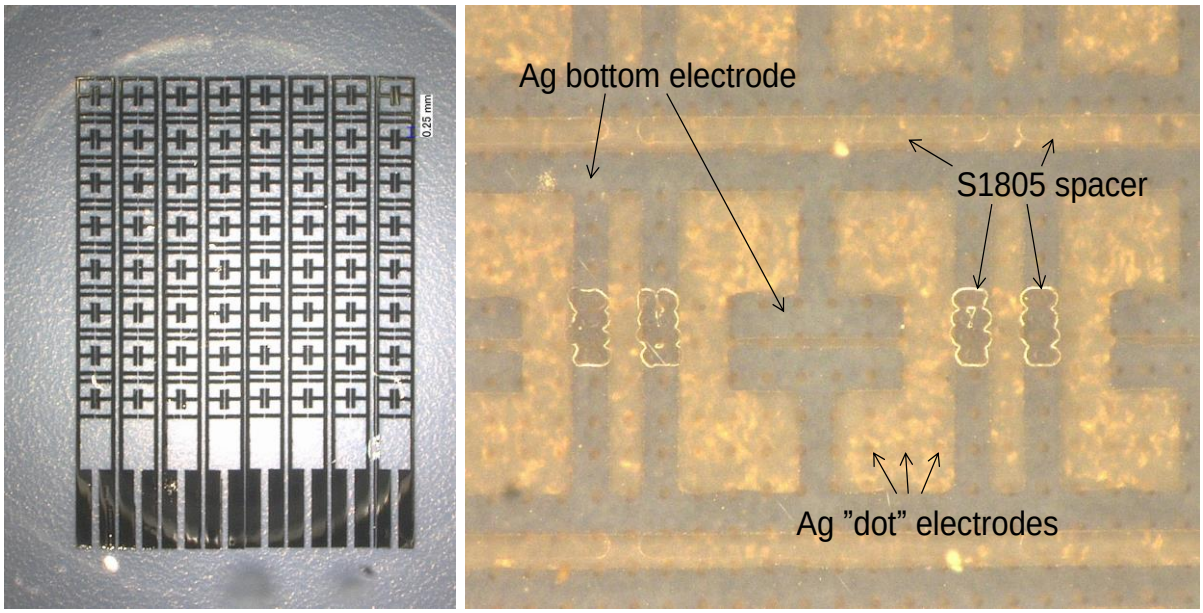

a) *b)*

***Figure 7**: Inkjet printed device for GHz range (design A2-GHz). SRR E MEMS device consist 16 unit cells (a). Bottom and top electrodes are Ag-nanoink. Top electrode consist 30 micrometers dots and spacer is 5 µm thick S1805 resist. Top electrode aligning is done using optical microscope (b).*

Based on the inkjet experiments and tests done using flexographic printing, we propose a following continuous roll to roll fabrication process for GHZ and THz MEMS devices (Figure 8). Manufacturing principle is based on combination of flexographic, inkjet printing and lamination.

Due to the high resolution a machine modification is needed and there are no existing tools available in the market. However experiments with table top tools shows suitability to this kind of manufacturing. To be apple to demonstrate this kind of manufacturing process a novel roll to roll tool need to build.

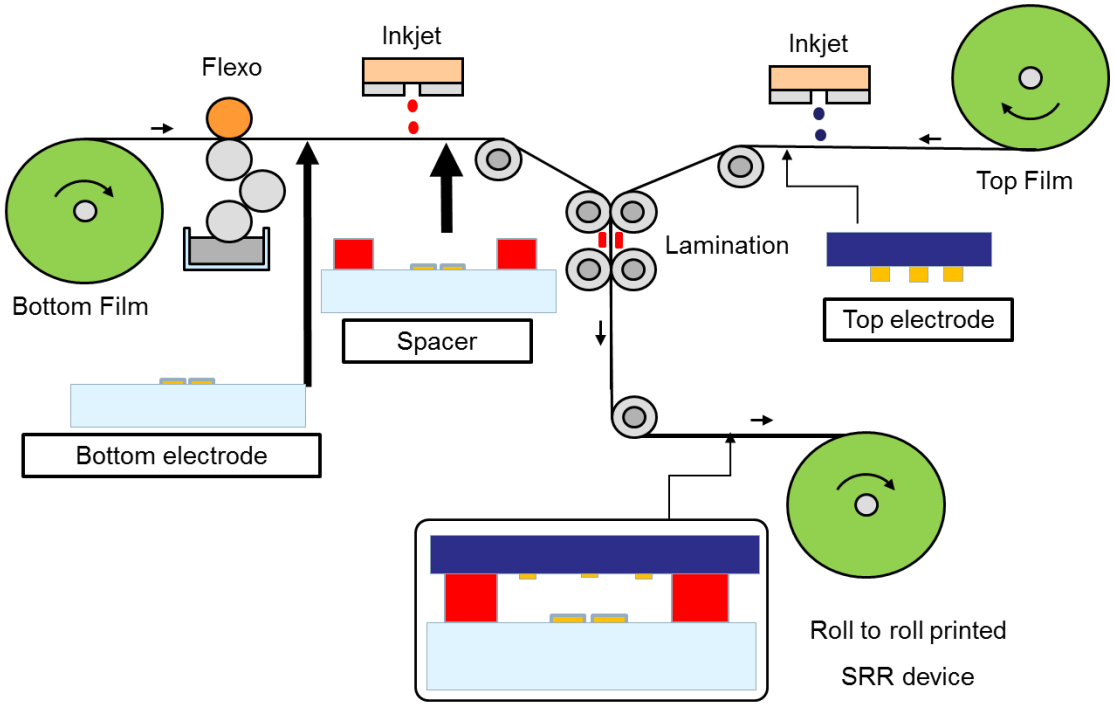

***Figure 8**. The roll to roll process includes patterning steps of the SRR and top electrode pattern following lamination step of top film onto substrate film. High resolution alignment is not needed.*

VTT-LIMMS-3. Smart Graphene Sensor

Markku Kainlauri visited Kawakatsu lab from September 2013 until March 2014. The work comprised of studying the fabrication of sharp Pt tips using electrochemical etching, graphene growth on Pt surfaces and process characterization.

Platinum tips were fabricated from 150 µm diameter platinum wire by electrochemical etching and polishing process. First tests on tip fabrication were performed at Kawakatsu laboratory by Dr. Pierre Allain prior to the visit of Mr Kainlauri. In order to test the CVD process in practise the first tips were sent to VTT for preliminary growth tests done using the RTP (rapid thermal processing) setup. Tip fabrication during the research visit was performed by Mr Kainlauri in collaboration with Mr Nishizawa.

The tip fabrication yielded tips with sufficiently sharp apex in the 10 nm range thus making Field Ion Microscopy feasible. The sharpest tips had a radius of curvature in the order of tens of

nanometers (Figure 9a) while most tips had a radius of curvature in the hundred nanometer range (Figure 9b). All tips were used for graphene CVD process testing regardless of their sharpness.

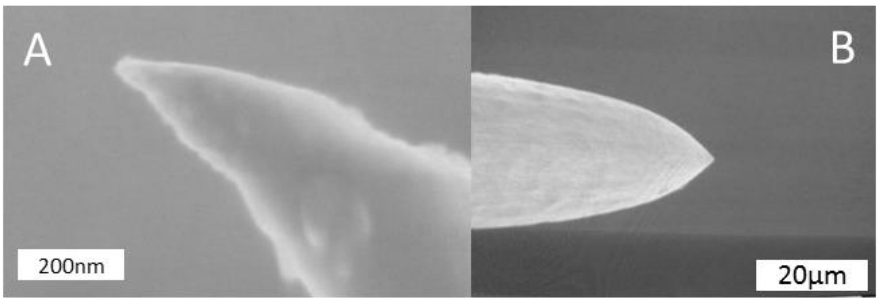

Figure 9. *SEM image of PT tips fabricated with the electrochemical etch method. Examples of sharp tips with optimised process a) having radius of curvature of 10 nm at the apex and tips with the unoptimised process b).*

Preliminary tests on the feasibility of graphene growth were performed using VTT Rapid Thermal Processing (RTP) chamber[6]. Pt tips fabricated at IIS Kawakatsu laboratory (Dr. Pierre Allain, Mr Hidenobu Nishizawa) were used to test the feasibility of growing graphene on Pt tips. Based on a process for growing graphene on planar, sputtered Pt thin films on Si wafer already in use at VTT, suitable process parameters for growth were already determined. However, as seen in Figure 10a, which shows the SEM images of Pt tip after a test run performed at 950 °C, too high temperature causes deformations to the thin tip apex. As a solution to the problem, a lower temperature of 850-900°C should be used. Graphene features typical to CVD deposited graphene on Pt were observed on Pt surface (Figure 10b).

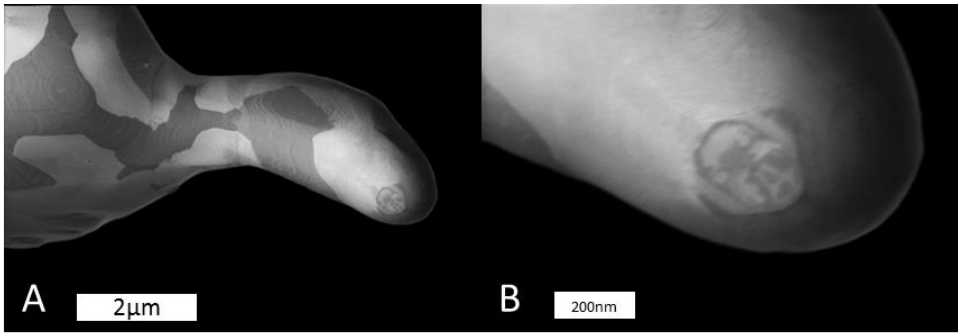

Figure 10. *Graphene deposition results from first tests done using the RTP setup at VTT. Distinct graphene features can be seen in the tip body a) and apex b). Tip deformation was due to too high temperature during the process.*

Tests done on graphene growth on the modified tube furnace setup showed the possibility to deposit graphene on Pt surfaces and Pt tips. Graphene layer growth was verified with TEM imaging. Several process runs were done to find out suitable process parameters for the use of the tube furnace for the growth of graphene on a platinum surface. Process optimisation was done by tuning the deposition pressure, time and partial pressures of the precursor gases. Based on previous experience and literature references temperatures of 800 and 850 °C were tested[7]. Increasing the temperature further would increase carbon solubility in platinum resulting in multilayer graphene

formation[8] and possible tip deformation as seen in preliminary graphene deposition tests performed at VTT. Pressure during pre-deposition anneal of Pt was tested between 140 Pa – 1200 Pa. Total pressure during the growth cycle was tested between 50 Pa – 320 Pa. Partial pressure ratio of the Ar/H_2 mixture to hexane vapour was between 30 and 2 during graphene growth. Process runs were also conducted with only Ar/H_2 precursor gas to get reference data. Final process parameters were adjusted to a temperature of 850°C with a pre deposition anneal in Ar/H_2 ambient at 300 Pa for 20 min followed by graphene deposition with partial pressures of Ar/H_2 and Hexane being 300 Pa and 20 Pa respectively giving a mixture of 6.3 % hexane.

TEM imaging of Graphene coated Pt tips was performed at IIS Kawakatsu laboratory with the help of Dr. Pierre Allain, and Master students Mr Shun Takeda and Mr Yuya Kumata. The TEM microscope at IIS Kawakatsu laboratory was JEOL UHV TEM/AFM capable of up to 200 kV imaging. Figure 11 shows the existence of a layer on top of the Pt tip, which is expected to be multilayer graphene.

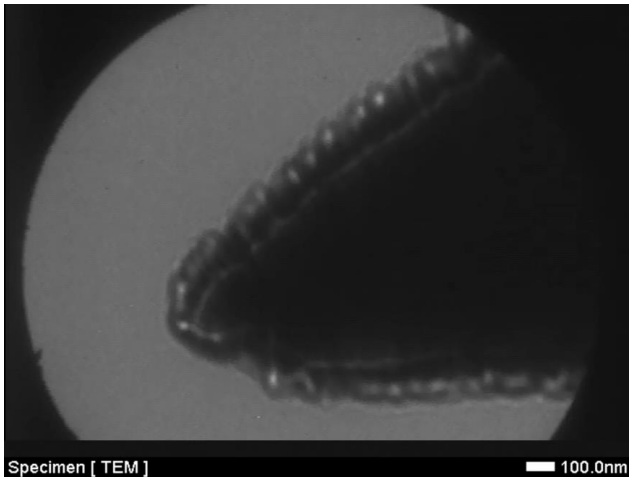

Figure 11. *TEM Image of a Pt tip with multilayer graphene coating.*

Method of growing graphene on a sharp Pt tip in an oscillatory form, as in the form of a cantilever, has yet to be studied, since graphene may easily attach itself to the curved surface during possible charge up in the growth process. Graphene coated Pt tips could additionally be used as substrate to immobilize biomolecules, either individual or monolayers, which could enable for them to be studied using microscopy methods such as FIM or STM. In conclusion, this work enables further studies of the feasibility of characterising graphene and related materials with the FIM/FEM method.

VTT-LIMMS-4. TEM analysis on AlN thin films

Tommi Suni worked at Fujita lab from March 2014 until May 2014. Despite that there were some equipment and sample related problems, we were able to prepare about 40 TEM samples with FIB (typical preparation time 4-10h/sample) as well as study 20 of those in TEM. Etching too much (no AlN remaining), bad contact to mesh (sample detached during transfer) and dropping of the mesh (one mesh containing 4 samples) were the reasons for losing half of the samples.

From the 20 samples observed, over 500 TEM images were taken. On low magnification images all the layers were well visible and on some of the high magnification images we could see the lattice planes of AlN. However, as we could not see the interface between the seed layers and the AlN, it was difficult to judge if there was amorphous layer and what might be its thickness at the beginning of the growth of the AlN film. This would had been the main information, as minimizing the non-crystalline part of the AlN film would improve the performance of the film for example in piezo-actuated MEMS devices. Based on our images taken near the interface, we believe that the quality of the AlN film is not fully crystalline or completely amorphous during the early stages of the deposition. We could measure the number of lattice planes in one image only in one case, which was for the old molybdenum on sample taken near the edge of the wafer. Then most of our pictures taken far from the interface show lattice planes in almost every case, which would indicate that the AlN quality is better after some first tens or hundreds of nanometers have been deposited. This is expected result, based on the literature.

6'' silicon wafers were used as start substrates. Before aluminium nitride deposition, five different seed layers (layer that will be below AlN) were chosen. Those were standard silicon wafer, highly doped silicon wafer, two different molybdenum layers (SiO2 under Mo) and AlN deposited on AlN, that has been surface treated. Target thickness for AlN was 1µm. After AlN deposition, the wafer was diced to get 1 cm x 1 cm pieces from it. As the stress of the films is different at the middle of the wafer than near the edge, samples to be observed were chosen so that from each wafer there would be a sample from the centre of the wafer as well as from the edge of the wafer. List of samples can be found from Table 1.

Table 1. List of samples

Seed layer	**Sample location**
Molybdenum deposited with older recipe	centre
Molybdenum deposited with older recipe	edge
Molybdenum deposited with newer recipe	centre
Molybdenum deposited with newer recipe	edge
Standard silicon	centre
Standard si	edge
Heavily doped Si	centre
Heavily doped Si	edge
Trimmed aluminium nitride film	centre
Trimmed aluminium nitride film	edge

We tried to do some calculations for the lattice planes and evaluate if there is big difference in the stresses of the films. However, as presented in previous chapter, we were not able to draw full conclusions. It was unfortunate that we could not see what kind of information we could achieve by using the scanning TEM originally meant for this work. But as this was not possible due to unfortunate tool breakdown, luckily there was FE-TEM for carrying the work. The authors would once more thank other Fujita lab members who postponed their studies with FE-TEM for allowing us to investigate our samples within the timeframe of the visit.

POTENTIAL IMPACT of VTT-LIMMS PROJECTS

EUJO-LIMMS activities has improved collaboration between partners and VTT. After this project is more easily to collaborate between EUJO-LIMMS partners. For example research exchange between partners are easy to make and partners choose EUJO-LIMMS universities and institutes rather than before. Bilateral project between individual European partners and LIMMS, has been positive effect EUJO-LIMMS has developed a visibility in Japan thanks to successful operation. Excellent research capabilities of EUJO-LIMMS will be radiated into the partner institutions beyond the research groups and the research networks between partners. The involvement of European partners in EUJO-LIMMS will increase partnership between EU and Japan go further on the frontiers of knowledge in Micro and Nano technologies. Such activities has increasingly designed and operated from an international perspective on the world scene. Europe can take the international leading role that it could have, notably to respond to major challenges.

MESA+
INSTITUTE FOR NANOTECHNOLOGY

MESA+, Netherlands – LIMMS, Japan COOPERATION

MAIN S&T RESULTS/FOREGROUNDS of MESA+-LIMMS PROJECTS

In a first task, an ultra-thin liquid Transmission Electron Microscope (TEM) cell was fabricated in which the presence of liquid could be confirmed in-situ by electron energy loss spectroscopy (EELS). Gold nanoparticles down to 15 nm in size were successfully imaged using the device. This work has been presented at the International 2016 IEEE MEMS Conference in Shanghai. In a second task, arrays of sub-10 nm silicon quantum dots were fabricated, and significant progress was made on different strategies for deterministic contacting of InAs and Si quantum dots. Along these different research lines, objectives and a good basis for long term international collaboration between the different groups involved have, respectively, been formulated and established.

This work package of EUJO-LIMMS was divided in two sub-tasks; aims and research questions are listed per sub-task.

MESA+/LIMMS-1. Fluidic TEM visualization of nano-vesicles and bilayer membranes

The aim of this sub-task was to develop a device for TEM imaging in the liquid phase, providing high resolution for the detection of small objects, and eventually of objects with poor contrast, as requested for biomolecular studies

The main questions to be answered in this sub-task were:

a. Can we realize a liquid TEM cell allowing imaging of specimens without any destructive preparation procedure?
b. Can we confirm the presence of liquid in the TEM cell?
c. Can we enhance the imaging resolution by decreasing the substrate thickness without endangering the lifetime of the device?
d. Can we eventually image biological objects which exhibit a poor contrast for TEM?

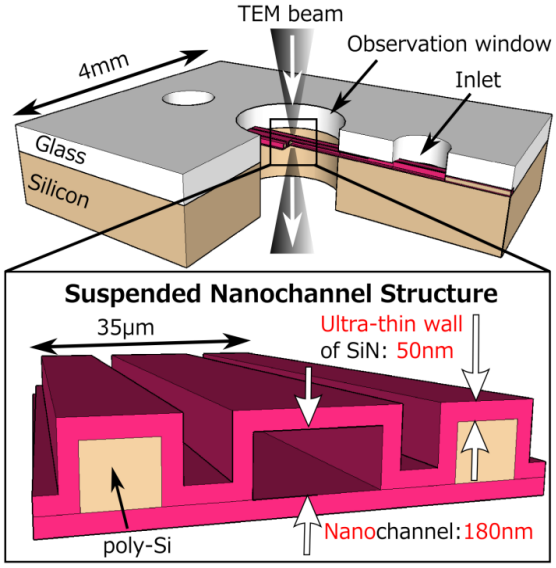

Figure 1: Schematic representation of the nanochannel-based liquid TEM cell.

A novel monolithic design was proposed to realize a nanochannel-based liquid TEM cell fulfilling some of the aforementioned requirements. As depicted in Fig. 1, it consists of a silicon and a glass wafers separated by a thin structure of silicon nitride (SiN) housing a suspended nanochannel. This nanochannel has a height of 180 nm, and is delimited by SiN ultra-thin walls (50 nm) allowing high-resolution imaging. An observation window is created in the glass substrate to focus the TEM beam in the nanochannel where imaging takes place, as well as two accesses for introduction of liquid and the samples to be imaged. This liquid TEM cell can be used without any modification with the STEM (Hitachi HD 2300, Hitachi Lt., Japan), and can be used with commercially available chip-holders.

The device was utilized for imaging experiments, using gold nanoparticles in liquid. A key-aspect to examine is the presence of liquid in the TEM cell, specifically in the suspended nanochannel. The presence of liquid can be confirmed using the technique of EELS (electron energy loss spectroscopy), which is made possible here through the use of very thin SiN walls.

Here, samples were loaded through one of the liquid inlets in the nanochannel, and they filled in the device by capillary action. As soon as liquid was seen to enter the channel, the device was entirely sealed using UV-curable glue.

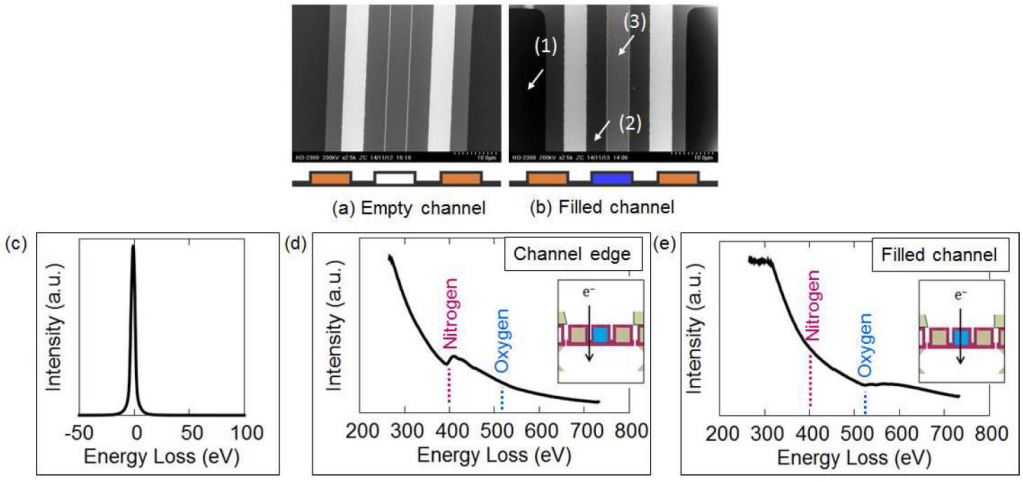

Figure 2: EELS measurements in the liquid TEM cell. (a,b) Z-contrast STEM images of empty and liquid-filled devices. EELS signals are recorded at different places, as indicated by the numbers. (c) Spectrum obtained in the vacuum area indicating zero-loss energy peak; (d) Spectrum obtained at the edge of the channel, showing the detection of nitrogen coming from the SiN material; (e) Spectrum recorded in the channel filled with solution, yielding a completely different trace than in vacuum, which confirms the presence of liquid.

After introduction of the sample, EELS measurements were conducted at different positions, as indicated on Fig. 2: (i) in the vacuum area, which is a negative control and used for calibration; (ii) at the channel edges containing only SiN; and (iii) in the liquid-containing channel. The contrast obtained between the empty and the filled channel strongly suggests the presence of liquid in the sample nanochannel, which is also confirmed by a distinguishable peak for oxygen.

The last step here was to image nanoparticles in the nanochannel, with the ultimate goal to characterize the imaging resolution with our liquid TEM cell. For that purpose, we used gold nanoparticles with a size of 10-100 nm that were introduced in the device as previously described. Figure 3 presents a typical image obtained for a nanoparticle sample with a nanoparticle size of ca. 15 nm in the device, as well as a graph showing the color intensity and confirming the size of the object. From this graph, the calculated resolution is 7.8 ± 3 nm (n= 20). Figure 4 presents images obtained for a sample with nanoparticles of 100 nm in size, moving in the liquid TEM cell, which again confirms the presence of liquid in the TEM cell.

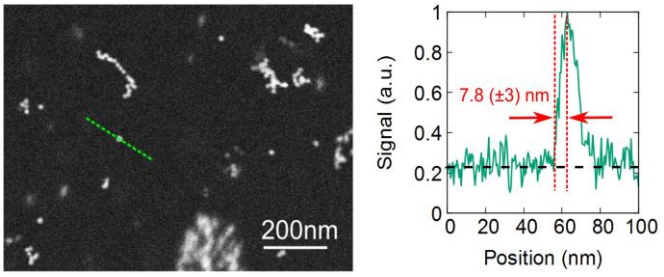

Figure 3: Gold nanoparticle (ca. 15 nm in size) imaging in the liquid TEM cell. Left: TEM image showing the gold nanoparticles; and right: color intensity spectrum confirming the size of the gold nanoparticle around 15 nm and showing a resolution of 7.8 ± 3 nm (n= 20).

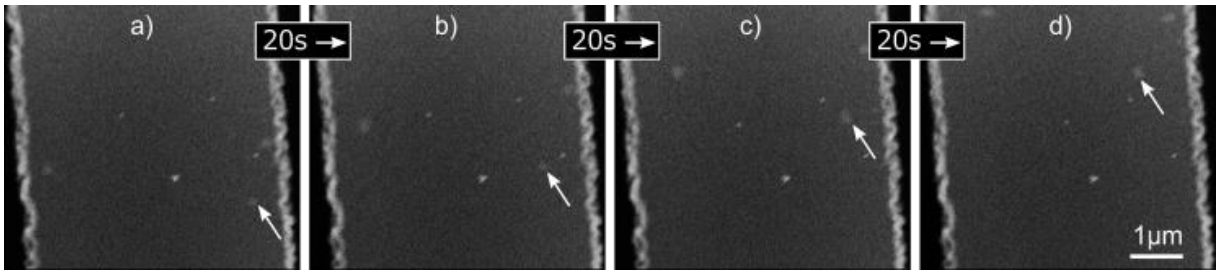

Figure 4: Gold nanoparticles (100 nm in size; indicated by the white arrow) moving in the TEM cell; pictures are taken with 20 s apart.

On-chip bilayer lipid membrane (BLM) formation

First test with a new device for on-chip BLM have been performed. Details of this work cannot be given here in the light of possible IP protection.

MESA+/LIMMS-2. Development of quantum-electro-optical transducers

The overall aim of this task is to fabricate, connect, and characterize individual quantum dots in the electro-optical domain, for future sensing, computation and energy harvesting applications.

The main questions addressed in this sub-task were:

a. Can we fabricate sub-10 nm Si quantum dots (QD's) by top-down fabrication schemes on wafer scale?

b. Can we detect the photoluminescence spectrum of these QD's?

c. Can we connect QD's on an individual level?

d. Can we perform photon assisted tunnelling experiments in these QD's?

Silicon QD fabrication

As a first step in Si QD fabrication we aim at top-down machining procedure (i) that is easily scalable to the size regime where quantum confinement effects can be expected, and (ii) that can produce high density arrays, because in optical (fluorescence) characterization experiments the expected quantum yield is rather low. The proposed fabrication process integrates the previously developed procedure for tetrahedral Si nanocrystal (NC) machining [Berenschot2009] with high density lithography procedures, in particular electron beam lithography (EBL) and displacement Talbot lithography (DTL).

The fabrication process builds on a combination of relative simple wet etching steps, with thermal oxidation of silicon, and low-pressure chemical vapour deposition (LPCVD) of silicon nitride. The first (DTL) lithography step is used to produce a high density array of V-grooves, covered by silicon nitride and a thin layer of silicon oxide on top of the silicon nitride. Subsequently, EBL is applied perpendicular to the groove pattern, followed by a sequence of (3D) etching steps in combination with retraction of the silicon nitride and LOCOS to produce a 3D-mask pattern (fig. 5).

High density arrays of Si NC (tetrahedra) have been successfully fabricated across areas of several square micrometers. Fig. 6 and fig. 7 show an overview and zoom-in of part of the fabricated NC array. The typical size of the fabricated NC's reached during the course of the project is around 10 nm. For the long term aim of having quantum confinement effects, we need to downscale this to 5 nm or slightly below. Due to intrinsic inaccuracies in the sequence shown in fig. 3, it is difficult to directly reach this small size. We envision add-on steps such as repeated oxidation/HF etching and self-limiting oxidation (limited by compressive stress building in the Si NC during oxidation) to accurately reach the 5 nm dimension.

The authors of this report are currently preparing a publication about the high density Si NC fabrication procedure developed during the project.

Reference:

[Berenschot2009] Berenschot, J.W., et al., *Chemically anisotropic single-crystalline silicon nanotetrahedra.* Nanotechnology, 2009. **20**(47): p. 475302.

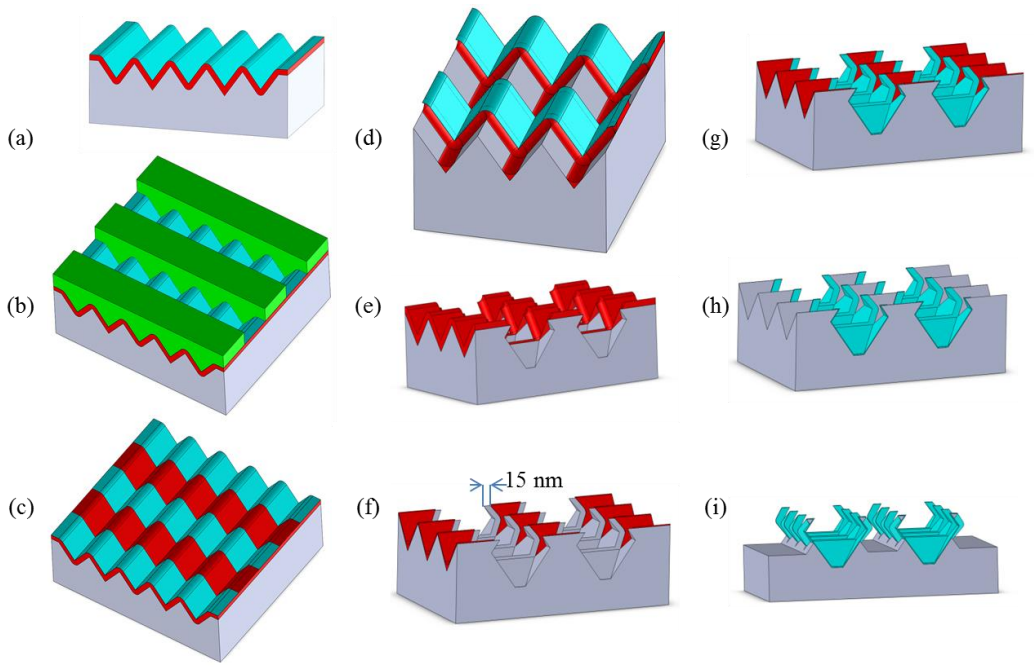

Figure 5. Schematic of the Si nanocrystal fabrication. (a) Doubled V-grooves with Si3N4 and SiO2 layer; (b) EBL lines 90˚ rotated with respect to the V-grooves; (c) Etching of SiO2, removal of EBL resist followed by patterning of the Si3N4 layer by corner lithography (d); (e) Removal of remaining SiO2 and anisotropic etching in KOH; (f) Retraction of Si3N4 by edge lithography; (g) LOCOS; (h) Selective etching of Si3N4; (i) Anisotropic etching in KOH creating silicon nanocrystals.

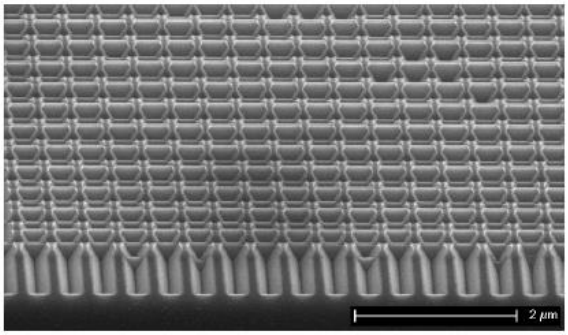

Figure 6. *SEM image of a grid of QD's. The spacing between the arrays is 200 nm. Courtesy of Erwin Berenschot and Janine Wilbers.*

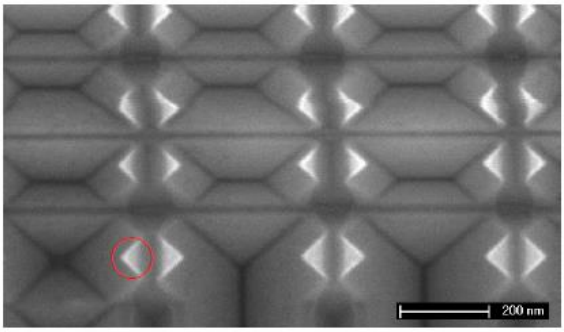

Figure 7. *Zoom onto the QD's, which are located in the tip of the brighter triangles, circled in red. Note that the QD's are not visible due to their size (Order of 10 nm). Courtesy of Erwin Berenschot and Janine Wilbers.*

Contacting Individual QDots and Opto-Electronic Characterization

High density arrays of single-crystalline silicon quantum dots have been fabricated by combining chemical anisotropic etching with nano-photolithography and electron-beam lithography, as described in the previous section. The quantum dots have been miniaturized to a sub-10 nm dimension in an attempt to realize a (quasi) direct band gap through quantum confinement. The goal was to optically characterize these quantum dots and attempt to solve the problem associated with the silicon substrate, which will most likely dominate the emission spectrum. Initial measurements confirmed the dominant nature of the silicon substrate emission. In the first experiment, the quantum dots were deposited onto a Ge substrate by ultrasonic dispersion. A spectrum showing a possible signature of the quantum dots was obtained from this sample. The second experiment was to encase the quantum dots in parylene C and remove this layer from the substrate. Parylene C is transparent and colorless in the visible regime, meaning it could possibly allow the quantum dots to be measured without much interference. However, photoluminescence measurements only showed emission from the parylene.

Terahertz (THz) waves can be a powerful tool to investigate the electronic properties of nanostructures, since many of these structures have electronic excitation energies which correspond to the THz wavelength. Nanostructures such as quantum dots have generated much interest for their potential important roles in electronic devices such as qubits and single-electron transistors. Indium arsenide (InAs) quantum dots exhibit some unique characteristics which make it a great candidate for research purposes. However, for device application and larger scale manufacturing, silicon could be more attractive because of its availability and its compatibility with current fabrication

processes for electronic devices. THz spectroscopy of InAs QDs on a gallium arsenide substrate is investigated, and the possibilities of using silicon for similar experiments are explored.
The formation of a break-junction by controlled electro-migration (EM) was investigated. While the creation of junctions around QDs was sometimes successful (fig. 8), breaking the junction by controlled EM was a challenging step for the short duration of this sub-project.

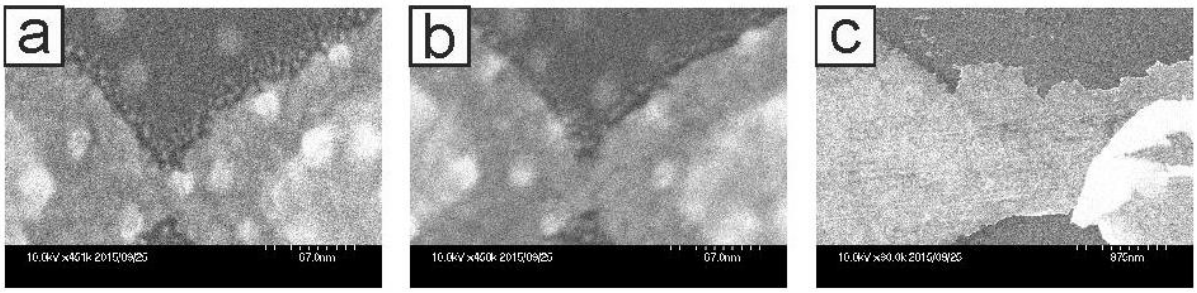

Figure 8. *Three SEM images of junctions resulting from the fabrication process. All devices are found on the same chip. (a) A QD (bright dot) can be seen in the middle of the junction, and seems to have a good chance to be between the two electrodes after electro-migration. (b) No QD seems to be in the middle of the junction, so that no working device can be expected. (c) The lift-off process was unsuccessful for this device, resulting in a large area of metal at the position of the junction.*

For the deterministic electrical contacting of InAs QD's we explored different paths.

First, the process of electro-migration was tested for existing samples. It turned out to be difficult to perform EM on the Au-Ti leads on the GaAs substrate. The conductivity was very low for this sample, in the order of 10−3 □ or below. This is indicative of the poor connections on the sample, which are likely caused by some dirtiness or oxidation between the EBL patterned leads to the PL patterned leads and/or the gold wire from the PL bond pads to the chip carrier. Furthermore, the conductivity showed an unexpected upturn as the bias voltage was increased during the EM process as well as a sudden breakage of the junction. Because of this, the samples from this batch were not investigated further.
The next step involved testing a method of aligning electrodes to quantum dots using bit marker structures (fig. 9) and SEM. As seen from the results the alignment was successful, with a deviation of ±15 nm in both the x- and y-directions, meaning that even small quantum dots could be contacted successfully with this method. Unfortunately, the SEM damages the quantum dots if exposed directly. Protection with PMMA proved fruitless, as the PMMA is burnt by SEM and no longer dissolves in a regular solvent as it should. Using 100 monolayers of AlO as a coating and a HF etch afterwards damaged the quantum dots as well, as the InAs is etched as soon as the AlO degrades.
Lastly, the AFM was used to avoid any damage to the sample during the mapping stage. There is some shearing in the images when compared to the original mask, which makes the position of the quantum dots uncertain in the middle of the image. Since the shearing seems to be only occurring in the vertical direction, only quantum dots that are near the top or bottom bitmarkers were contacted. Similar to the SEM the alignment was good (fig. 10) with an approximate misalignment of ±15 nm as well, with a successful contact yield of just over 60% for this particular sample. The junctions were not electrically characterized yet as the fabrication process took longer than expected to finish.

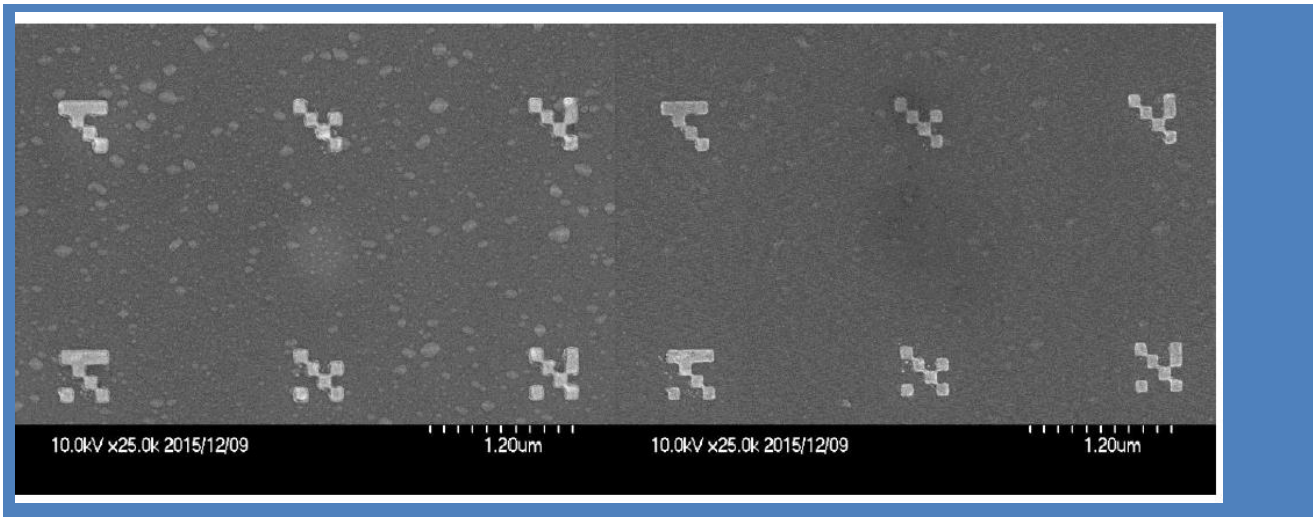

Figure 9. *Bit mark patterns for alignment of QD's with electrodes.*

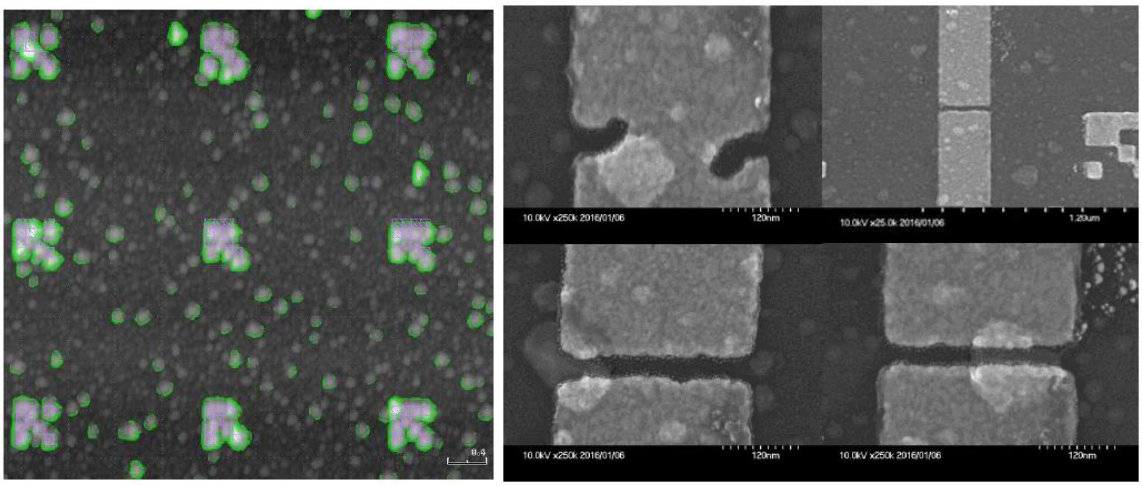

Figure 10. *Left: AFM image (Tokyo) aligned to mask. Scale is 0.4 µm. Right: Selection of representative junctions: Fused, empty and contacted.*

POTENTIAL IMPACT of MESA+/LIMMS PROJECTS

One of the long term goals of the liquid TEM cell concept developed in task 8.1 is to study biomolecular processes, including biomolecular interactions with and transport through bilayer lipid membranes (BLMs). Imaging such molecular interactions, which requires high resolution approaches in the liquid state, is extremely important in the biomedical research field, to elucidate molecular processes at the cell surface, and for this, artificial BLMs which are widely used as models for the cell membrane, are ideally suited. Such interactions play a key role for instance in neurodegenerative diseases, and transport phenomena through the cell membrane are equally important for drug delivery applications as well as for (nano)toxicity studies.

Another activity in task 8.1 has focused on the development of a new nozzle device for lipid bilayer vesicle generation. When successful, such devices could find application in efficient and controlled encapsulation of drugs for the cost-effective production of homogeneous and well-characterized nanomedicines, e.g., for cancer treatment. In part II of this report we address this opportunity more in detail.

In task 8.2 we have been working towards the electrical connection of arrays of QD's on an individual level. When successfully connected, silicon QD's could be a component in future efficient photovoltaic devices. They are being explored for so-called multiple-exciton generation, which is one way to utilize the full solar spectrum in a more efficient way.
Another important long term application is the realization of electrically driven single-photon sources in silicon. Single-photon sources are highly important for optical quantum communication and computing schemes. Quantum dots are very sensitive charge sensors. By incorporating a QD in a nanofabricated tip, it could be applied as a very sensitive scanning charge sensor.

Altogether these examples show that the project contributes to some major socio-economic developments, including the transition to renewable energy and disruptive information technologies, as well as progress in medical science and technology.

EUJO-LIMMS, First EU Laboratory in Japan: SUMMARY of IMPACT

EUJO-LIMMS activities provide a significant achievement to improve the collaboration of the 4 European partners - EPFL, IMTEK, MESA+,VTT - in Japan as part of the European Laboratory lead by CNRS and The University of Tokyo. Above this primary goal, the 4 EU partners have reached increased visibility in Japan to further develop their international links and have locally in Tokyo established additional collaboration between them. It was witnessed by the 4 EU partners that excellent research capabilities of EUJO-LIMMS are radiating into the partner institutions beyond the research groups and the research networks between partners. The involvement of European partners in EUJO-LIMMS established a unique partnership between the European Union and Japan and met its goal which was to push the frontiers of knowledge in Micro and Nano technologies.

Significant results have been obtained in the field of Nano and Micro fabrication. For low cost and affordable process, the joint work between IIS, EPFL, IMTEK and VTT allow to develop breaking new approach to advanced 3D Micro / nanofabrication techniques. A ensemble of 4 methods was investigating based on thermal scanning probe lithography (TSPL), advanced stencil lithography, micrometre-size moulding and Roll to Roll (R2R) technologies. These technologies allow replicating devices very small features sizes without the requirement of expensive equipment and dedicated specialized operators, or in the case of R2R technique for very large-scale replication. These advanced processing techniques have been demonstrated for cell captures, neuron growth and patterning of high performance triboelectric generator based silk fibroin and for GHz MEMS metamaterial filter. These new capability bring advanced patterning and so the advantage of microsized structuration far beyond the sole silicon based nanoelectronic towards new material and new application. More heterogeneous integrations are possible as cell and electronics interface and integration of new material for new approach in computing or energy monitoring.

Relative to Nanotechnology, the combination of the expertise between Japanese and EU partners allow combining advanced nanotechnology mostly developed in EU with unique measurements capabilities in IIS. VTT provides sample with advanced coating capability for Graphene and AlN films. These new processes was evaluated with UTokyo-IIS researchers with advanced and dedicated Atomic Force Microscopy (AFM) technique and unique MEMS platform installed in Transmission Electron Microscope (MEMS in TEM). These successful research approach was extended with MESA+ that provided “corner” technology for the realization of micro fluidic chamber with nano sized membranes and electronic and photonic quantum dots. This new concept was established in EUJO-LIMMS for wide scientific area, as attested by the 4 topics: single atomic layer deposition capability, nano sized graphene based oscillator, opto-electronic quantum dots and nano fluidic. This unique complementary expertize links the nanotechnology development and its in-situ evaluation, so bringing breakthrough approach for a better assessment of nanosized devices properties and its further optimization.

The third main impact is related to to BioMEMS, the fusion between micro and nano technology and the biology and medical field. In EUJO-LIMMS we successfully tackled the bioMEMS

technology with various sizes range to open wide application opportunities. The real time visualisation of biomolecular process was investigated with MESA+ nano fluidic devices that were brought in IIS MEMS in TEM capability. With IMTEK and EPFL, new in vitro cell culture capabilities were develpped with micro sized patterning of microfluidic devices; oriented cell growth for neuron or high throuput cell capture and growth were successfully demonstrated. At a multi cell level, VTT and IIS fabricated a microfluidic device to mimic human body and used it to test an influence of a prodrug on cancer cells. Finally IMTEK and IIS established advanced method for interconnecting rigid miniaturized probes to flexible cables and for temporarily stiffening the resulting flexible structures using biocompatible polymers. This technology achievement provides novel technology and great improvement in smart intracortical neural probes for neuroscience. With this 4 example ranging from the molecular sized until intracortical, EUJO-LIMMS pushes the bioMEMS application opportunities towards new biological and health care potential like drug effect analysis (Molecular reaction visualisation, organ on chip), drug screening (high throughput cell arrays) and Neuroscience (neuron chip and neural probe).

Through these scientific activities, Europe can take a leading role on the international scene by responding to major challenges in which Micro and Nanotechnology are playing a key role for biology, medical application, communication and energy.

All information about the project and scientific results are on the EU Laboratory's **website:** **http://limmshp.iis.u-tokyo.ac.jp/**

The EUJO-LIMMS project gratefully acknowledges the European Union's funding under the 7th Framework Program, Grant Agreement number 295089.